A Standardized Set of MoClo-Compatible Inducible Promoter Systems for Tunable Gene Expression in Yeast

Richard O'Laughlin,*,[#] Quoc Tran,[#] Andrew Lezia,[#] Wasu Ngamkanjanarat, Philip Emmanuele, Nan Hao, and Jeff Hasty*

ACCESS | Metrics & More | Article Recommendations | Supporting Information

ABSTRACT: Small-molecule control of gene expression underlies the function of numerous engineered gene circuits that are capable of environmental sensing, computation, and memory. While many recently developed inducible promoters have been tailor-made for bacteria or mammalian cells, relatively few new systems have been built for *Saccharomyces cerevisiae*, limiting the scale of synthetic biology work that can be done in yeast. To address this, we created the yeast Tunable Expression Systems Toolkit (yTEST), which contains a set of five extensively characterized inducible promoter systems regulated by the small-molecules doxycycline (Dox), abscisic acid (ABA), danoprevir (DNV), 1-naphthaleneacetic acid (NAA), and 5-phenyl-indole-3-acetic acid (5-Ph-IAA). Assembly was made to be compatible with the modular cloning yeast toolkit (MoClo-YTK) to enhance the ease of use and provide a framework to benchmark and standardize each system. Using this approach, we built multiple systems with maximal expression levels greater than those of the strong constitutive *TDH3* promoter. Furthermore, each of the five classes of systems could be induced at least 60-fold after a 6 h induction and the highest fold change observed was approximately 300. Thus, yTEST provides a reliable, diverse, and customizable set of inducible promoters to modulate gene expression in yeast for applications in synthetic biology, metabolic engineering, and basic research.

KEYWORDS: *inducible promoter, chemically induced proximity (CIP), modular cloning (MoClo), toolkit, auxin, yeast*
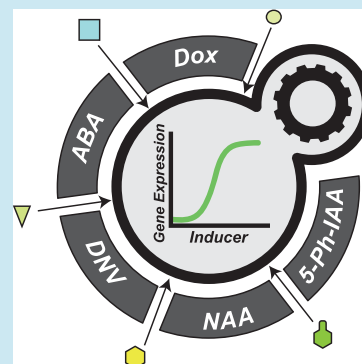
INTRODUCTION

Inducible promoters are versatile and widely used molecular tools. By allowing gene expression to be extrinsically and dynamically controlled, these systems can be applied to perturb endogenous regulatory networks[1,2] and build complex genetic devices.[3,4] Inducible promoters for *Saccharomyces cerevisiae* include[5] a number of native and non-native systems that are responsive to small molecules;[1,6−11] however, many have significant drawbacks that limit their utility. While native promoters such as *pGAL1* and *pCUP1* are often used[12] to control downstream genes with galactose[13] or copper,[14] respectively, the use of nutrients as inducers can lead to unwanted pleiotropic effects on cellular physiology.[15,16] Likewise, although bacterial repressors can be used to create inducible systems in eukaryotes by blocking transcription from constitutive promoters in the absence of small molecules that inhibit their DNA binding activity to operator sequences,[7,8,17,18] these systems are challenging to tune and can have high basal expression levels. Despite recent work by Chen et al.,[7] which expanded the ability of bacterial repressors to function in yeast, many accessible and broadly used inducible systems in *S. cerevisiae* still employ synthetic transcription factors with both DNA binding (DB) and transcriptional activation (TA) domains that turn on gene expression from synthetic minimal promoters.[2] These systems include two categories: Inducer-

OFF activators, which initiate gene expression in the absence of inducer, and Inducer-ON activators, which initiate gene expression in the presence of inducers.

In yeast, multiple Inducer-OFF and Inducer-ON systems have been made with components from bacteria, viruses, and human cells. Fusing bacterial repressors such as TetR or PhlF to one or more repeats of the herpes simplex virus VP16 TA domain produces Inducer-OFF activators where gene expression is inversely correlated with the level of tetracycline or doxycycline (Dox)[19,20] and 2,4-diacetylphloroglucinol (DAPG),[6,8] respectively. The Dox-responsive system, referred to as Tet-Off, was one of the earliest systems of this kind, and its transcription factor is known as the tetracycline transactivator (tTA).[20] Through mutagenesis-based approaches,[19] Inducer-OFF activators that use bacterial repressors as their DB and inducer sensing elements have been converted into Inducer-ON activators. Notably, mutations to the TetR component of tTA resulted in the reverse tetracycline transactivator (rtTA) and

thereby Tet-On,[19,21] an Inducer-ON system where gene expression is activated by the addition of Dox, instead of by its removal. Recently, mutations introduced into two other bacterial transcription factors, PhlF and LuxR, have successfully yielded Inducer-ON activators responsive to DAPG and *N*-(*β*-ketocaproyl)-L-homoserine lactone (HSL), respectively.[6]

In addition to mutating bacterial repressors, it is also possible to create Inducer-ON activators via rational design by utilizing the natural functions of certain proteins. The yeast beta-estradiol-inducible systems[9−11,22] are prominent examples of the successes of this strategy. Here, transcriptional activators were engineered to be beta-estradiol inducible by fusing a human estrogen receptor between their DB and TA domains.[9−11,22] Binding of beta-estradiol to the receptor domain causes the synthetic transcription factor to translocate from the cytoplasm into the nucleus where it then activates gene expression.[11] This function mimics the natural ability of beta-estradiol to bind to and regulate the nuclear localization of proteins containing its hormone-binding domain in human cells.[22] As an inducible system in yeast, the beta-estradiol system has gone through multiple design iterations[9−11,23] and has been used in numerous applications.[1,9,24] In addition, a similar inducible activator responsive to the human hormone progesterone was recently made.[9] Together, these features further underscore the potential of the rational design approach in creating Inducer-ON activators and highlight how natural proteins or even synthetic systems originally designed for use in higher eukaryotes can be redesigned to function in yeast. However, further application of these approaches is needed, since improving existing inducible systems and creating new ones would be highly beneficial for several reasons.

First, some inducers of the recently reported Inducer-ON systems may be toxic to yeast at relevant concentrations. For the HSL-On[6] and DAPG-On[6,8] systems, their inducers, HSL and DAPG, have been shown to alter yeast budding patterns[25] and negatively impact mitochondrial metabolism and growth,[26] respectively, although these effects of DAPG have been mild in other studies,[8] despite it being an antifungal agent.[26] Second, as even seemingly benign molecules like Dox can impact cells,[19,27] there is an opportunity to expand the number of available Tet-On systems in yeast as several next-generation or advanced rtTA variants with greater sensitivities[19] have been reported for mammalian cells. Third, different inducers may be ill-suited for certain applications. For example, beta-estradiol and progesterone systems may not function within polydimethylsiloxane (PDMS) microfluidic devices, as PDMS rapidly sequesters hydrophobic molecules such as hormones.[28] Fourth, expanding the number of orthogonal inducible activators for yeast—thereby emulating earlier efforts in bacteria[29]—would enable small-molecule control of more individual genes and facilitate the construction of larger genetic circuits, which often use inducible promoters as "sensors" that act as inputs.[3,4,7] Finally, using and comparing different published systems is often complicated by a lack of standardization,[30] since disparate promoters, terminators, fluorescent reporters, genome integration sites, and yeast strains can be used for their construction and testing. For these reasons, it is clear that there is a need to increase both the quantity and accessibility of inducible promoter systems and that doing so would offer greater flexibility for yeast researchers to select the system that best suits their experimental needs.

Here, we address the shortcomings in available options for inducible promoter systems in *S. cerevisiae* by developing the yeast Tunable Expression Systems Toolkit (yTEST). By using the existing literature to identify cutting-edge inducible promoter systems for mammalian cells, we redesign several of them to achieve robust performance in budding yeast. These include four classes of systems consisting of advanced rtTA variants regulated by Dox, as well as inducible promoters regulated by abscisic acid (ABA), a plant hormone,[31] danoprevir (DNV), an antiviral compound,[32] and 1-naphthaleneacetic acid (NAA), a synthetic variant[33] of indole-3-acetic acid (IAA), which is part of the auxin class of plant hormones.[34−36] Furthermore, we applied the design principles learned from these efforts to engineer a new inducible system for yeast that has not yet been developed for mammalian cells that utilizes 5-phenyl-indole-3-acetic acid (5-Ph-IAA)—another synthetic auxin variant—[37] as an inducer, thereby bringing the total number of inducible systems in yTEST to five. In order to enable wider use and application, we performed detailed quantitative characterization of the induction properties of each system and utilized a highly modular cloning approach that expedited construction and customization. By increasing the number of inducible promoters for *S. cerevisiae*, yTEST can potentially facilitate new applications in molecular and synthetic biology.

■ RESULTS

A Modular Cloning Framework for Constructing Standardized Inducible Systems. To expand the catalog of inducible activators for budding yeast, we leveraged the comparatively larger list of these systems created for use in Chinese hamster ovary (CHO) or human cells. As previously mentioned, several new rtTA variants with improved basal and maximal expression levels[19] are now frequently used in mammalian cells, although, to our knowledge, many of these new variants have not been systematically tested in yeast. Indeed, this is also true of many novel Inducer-ON systems recently developed for mammalian cells, which use small molecules such as ABA,[38−40] caffeine,[41] rapamycin,[42] DNV,[32,43] and auxin/IAA[34] to control the association of DB and TA domains of synthetic transcription factors, a strategy known as chemically induced proximity (CIP).[44] Given the functionality and robustness demonstrated by these systems in higher eukaryotes, we set out to systematically and quantitatively test their effectiveness in budding yeast. Since caffeine and rapamycin are known to inhibit growth in *S. cerevisiae*,[45] we focused on creating Dox-inducible systems with three of the most advanced rtTA variants, as well as ABA-, DNV-, and auxin-inducible systems.

To optimize these systems for yeast, we utilized the modular cloning (MoClo) yeast toolkit (YTK) made by Lee et al.[12] The MoClo yeast toolkit, or MoClo-YTK, contains a diverse set of eight different categories of parts—including constitutive promoters, terminators, and plasmid backbones—that are referred to as Types, and each contain unique 4 bp overhangs that enable them to be combined via the Golden Gate reaction-based modular cloning system.[46] Furthermore, new parts can be formatted in this way and used interchangeably with other parts in the kit, enabling the creation of entirely new MoClo-YTK-based kits for specific applications, such as the Yeast GPCR-sensor Toolkit made by Shaw et al.,[23] which provides parts for engineering GPCR signaling networks. Thus, MoClo-YTK provides an expandable foundation that enables rapid cloning, testing, and troubleshooting of customizable genetic constructs—ideal features for creating and tuning novel inducible promoter systems.
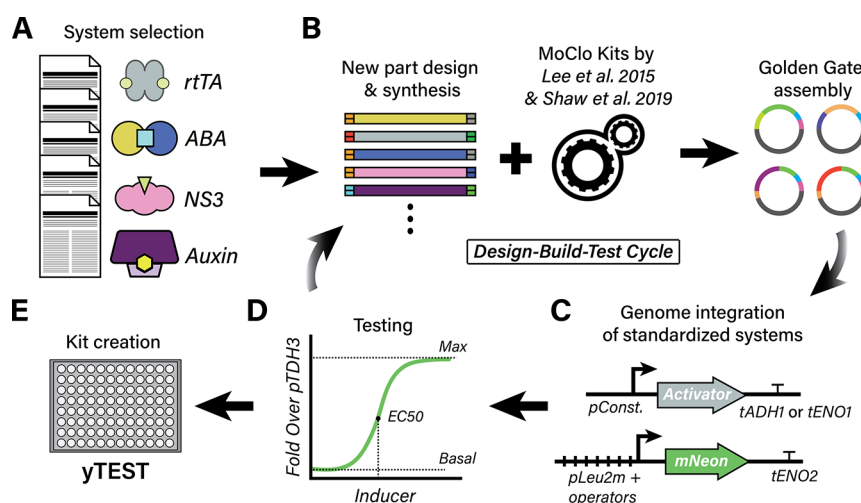
Figure 1. Workflow for developing yTEST. (A) Candidate inducible promoters were identified in the literature from recently reported mammalian cell systems. Three advanced rtTA variants, the ABA system, the NS3 system, and the auxin system, were selected for testing in yeast. Dox, abscisic acid, danoprevir, and 1-naphthaleneacetic acid (a synthetic auxin), respectively, are the small molecules that control these systems. (B) Parts for each system were yeast codon optimized, formatted as the appropriate MoClo-YTK part type, and synthesized. New parts were combined with existing MoClo-YTK parts (Lee et al.[12]) and parts from the Yeast GPCR-sensor Toolkit (Shaw et al.[23]), through Golden Gate assembly reactions to form cassette plasmids. (C) Each followed a standard format: constitutive promoters (*pConst.*) expressed the inducible activators, a minimal *LEU2* promoter[23] with operator sites (*pLEU2m*+operators) drove the mNeonGreen (mNeon) reporter gene, ADH1 or ENO1 terminators were used for cassettes containing activators, and the ENO2 terminator was used in mNeon reporter cassettes. All constructs were chromosomally integrated. (D) Promoters were tested in yeast using 6 h induction windows for each system, and induction curve properties were quantified. Induction fluorescence was expressed relative to *pTDH3*-mNeon-*tENO2*. Systems were improved via a design−build−test build cycle at this stage. (E) yTEST contains the validated parts, expression cassettes, and plasmids from this process.

Using MoClo-YTK as our basis, we sought a standardized approach for designing and benchmarking inducible activators. All components needed for the inducible promoters relying on Dox, ABA, DNV, and auxin were first identified from recently published work (Figure 1A). Following MoClo-YTK guidelines, we designed and created new parts needed for testing each of these three systems and then cloned them, along with other necessary parts from MoClo-YTK and the Yeast GPCR-sensor Toolkit, into cassette plasmids[12] (Figure 1B). We used a consistent design format for each cassette and integrated them into the genome (Figure 1C) in order to minimize variability and enable comparisons within and between the four systems after measuring the response of each to its inducer (Figure 1D). For analysis, fluorescence values were expressed relative to those of the *TDH3* promoter driving mNeon (*pTDH3*-mNeon-*tENO2*), as *pTDH3* is a commonly used strong promoter and Lee et al.[12] found it to be the strongest constitutive promoter in the MoClo-YTK. After testing and verification, all components needed to use these systems were aggregated to create yTEST and facilitate broader use (Figure 1E).

The individual parts included in yTEST consist of major protein coding and DB sequences that fall into the part Types 2A, 2, 3, 3A, 3B, and 4A. (Figure 2). As noted above, since yTEST was designed to work within the MoClo-YTK framework and alongside similar kits, complete assembly from individual parts of the three inducible systems described here also requires parts from MoClo-YTK and the Yeast GPCR-sensor Toolkit. Importantly, this includes the minimal *LEU2* promoter[23] (*pLEU2m*) from the Yeast GPCR-sensor Toolkit, which we use as the core promoter for each system, as Shaw et al.[23] demonstrated that *pLEU2m* exhibits superior induction properties compared to other minimal promoters, including the often-used *CYC1* minimal promoter.

Dox-Inducible Systems with Advanced rtTA Variants. The rtTA component of the Tet-On system has been in a continual state of improvement in mammalian cells. While Roney et al.[47] adapted the rtTA-M2 variant for use in yeast, which includes several mutations that improve its functionality relative to the original rtTA,[48] and produced multiple variants with mutations further enhancing its function, there has been no direct comparison among the most advanced systems used in mammalian cells. These principally include the variants rtTA3, based on work by Das et al.,[49] and rtTA-v10 (also known as Tet-3G[19]) and rtTA-v16 from Zhou et al.,[50] which contain different mutations and, in the case of rtTA3, different TA domains (Supporting Figure S1). Therefore, we set out to systematically test each of these variants in yeast and evaluate the trade-offs each provides in terms of sensitivity to Dox, basal expression, maximal expression, and fold change.

To tune each system, we placed rtTA3, rtTA-v10, and rtTA-v16 under the control of constitutive promoters of various strengths (Figure S2) and tested the induction properties of each configuration using *tetO7-pLEU2m* driving mNeon (Figure 3A). We started with the medium-strength constitutive promoter *pRPL18B* and found that all three systems showed increases in expression of the mNeon reporter as Dox levels increased (Figure 3B), as expected. The rtTA3 and rtTA-v10 systems exhibited relatively low basal expression levels in the absence of Dox that were 1.2 and 5.2 times higher than background levels in BY4741 strains without any fluorescent proteins (Figure 3E) and had maximal expression levels 0.9 and 1.6 times that of *pTDH3*-mNeon (Figure 3B,E,F), respectively. Meanwhile, the rtTA-v16 system exhibited both high maximal and basal expression levels, with even the fluorescence of the uninduced basal state nearly equal to the levels achieved by *pTDH3*-mNeon (Figure 3B,E,F). Indeed, similar results for this system were previously obtained in mammalian cells, where cells

rtTA systems	
Part	**Type**
rtTA3	3
rtTA-v10	3
rtTA-v16	3
tetO7-pLEU2m	2

Part from Yeast-GPCR Sensor Toolkit

Auxin systems	
Part	**Type**
amtRO7	2A
AmtR-NES	3A
AIDΔ34	3B
TIR1-U1	3B
TIR1-U2	3B

ABA systems	
Part	**Type**
phlfO7	2A
PhlF-NES	3A
ABI	3B
PYL1	3B

NS3 systems	
Part	**Type**
NS3-V1	3B
NS3-V2	3B
NS3a	3B
Linker-NS3a	3B
DNCR2	3B
LexA-NES	3A
lexAO6	2A
LexA-NLS	3A

Parts from Yeast-GPCR Sensor Toolkit

Reporter	
Part	**Type**
mNeonGreen	3
pLEU2m	2B

Part from Yeast-GPCR Sensor Toolkit

Activation domains	
Part	**Type**
NLS-VP48	3A
NLS-VP48-1XOaf1	3A
NLS-VP48-2XOaf1	3A
VP48	4A
NLS-VP48-2XOaf1	4A
VP48-2XOaf1	4A

Figure 2. Parts included in yTEST. The Dox-inducible systems consist of parts for several advanced rtTA variants (Type 3). A minimal *LEU2* promoter with seven repeats of the Tet operator sequence (tetO7) was used as the promoter (Type 2) for the rtTA systems and was originally designed by Shaw et al.[23] as part of the Yeast GPCR-sensor Toolkit. The abscisic acid (ABA)-inducible systems use Type 2A parts with seven repeats of the PhlF operator sequence (phlfO7), a DB (PhlF-NES) domain Type 3A part, and Type 3B parts for controllable heterodimerization (ABI and PYL1). For the NS3 systems, three variants were designed. Two variants use one of two Type 3B NS3 domains, termed NS3-V1 and NS3-V2. The third variant relies on CIP of Type 3B parts NS3a and DNCR2. Variants with and without a protein linker sequence on NS3a were tested. All three variants are inducible with danoprevir and use a LexA DB domain Type 3A part, either LexA-NLS, from the Yeast GPCR-sensor Toolkit by Shaw et al.,[23] or LexA-NES, both of which bind to a Type 2A part with six repeats of the LexA operator sequence (lexAO6, also from the Yeast GPCR-sensor Toolkit). For the auxin systems, choice of Type 3B parts TIR1-U1 or TIR1-U2 determines whether the system is inducible by NAA or 5-Ph-IAA, respectively. Both variants bind to AIDΔ34 (Type 3B) in the presence of an inducer, and both were tested using AmtR-NES (Type 3A) as the DB domain and a promoter with seven repeats of the AmtR operator sequence (amtRO7, Type 2A). Multiple activation domains (Type 3A and 4A) with various strengths and configurations were tested and used for the ABA, NS3, and auxin systems. We note that the NLS-VP48-2XOaf1 4A part does not contain a stop codon and is meant to be used with the *ADH1* terminator, which contains an early stop codon within it (see Supporting Information for more details on this part). For testing all systems, a Type 3 mNeonGreen fluorescent reporter was used and the Type 2/Type 2B *pLEU2m* from the Shaw et al. Yeast GPCR-sensor Toolkit[23] was used as the core promoter for all systems. Where noted, NLS and NES indicate nuclear localization and nuclear export sequences added to parts, respectively.

transiently transfected with nonintegrating plasmids exhibited high basal expression levels.[19] As a result, we decided to further test each of the three variants by increasing the strengths of the promoters expressing rtTA3 and rtTA-v10 and decreasing the strength of the promoter expressing rtTA-v16.

To accomplish this, we used *pTDH3* to drive rtTA3 and rtTA-v10 and weak promoters *pRNR2* and *pRAD27* to drive rtTA-v16. Using *pTDH3* led to only modest increases in maximal expression relative to *pRPL18B*: 19.7% for rtTA3 and 2.6% for rtTA-v10. However, this change in promoter had large effects on basal expression levels, which increased approximately 10-fold for rtTA3 and 2-fold for rtTA-v10 (Figure 3C,E,F). On the other hand, the use of either *pRNR2* or *pRAD27* in combination with rtTA-v16 substantially reduced basal expression levels for this system by more than 20-fold compared to when used with *pRPL18B* (Figure 3E). Furthermore, maximal expression levels remained high, with both promoters allowing rtTA-v16 to still achieve approximately 1.5× higher maximal levels than *pTDH3*-mNeon. In total, *pRPL18B*-rtTA3 resulted in the system with the greatest fold change, reaching maximal levels nearly 120 times that of its basal levels (Figure 3G). The *pRNR2*-rtTA-v16 and *pRPL18B*-rtTA-v10 systems also had high fold changes of 39- and 47-fold, respectively (Figure 3G). In terms of sensitivity to Dox, the rtTA-v16 and rtTA-v10 systems were able to respond to concentrations much lower than those of the rtTA3

systems (Figure 3H). The EC_{50} value for the most sensitive rtTA system (excluding *pRPL18B*-rtTA-v16), *pRNR2*-rtTA-v16, was 24.2 nM while the EC_{50} for the least sensitive system, *pRPL18B*-rtTA3, was 135 nM, a more than fivefold increase.

When considered together, the Dox-inducible systems described here offer a spectrum of choices, where systems with multiple induction properties can be utilized. For example, the highly Dox-sensitive *pRNR2*-rtTA-v16 system would likely be most useful for applications requiring prolonged continuous induction, such as replicative aging experiments, which are carried out over the course of several days in microfluidic devices,[51,52] in order to limit the amount of Dox cells are exposed to while still offering tight control and strong maximal expression. Alternatively, *pRPL18B*-rtTA3 would be preferred when limiting basal expression is paramount, such as in cases where even low levels of a gene can produce a large effect. As an example, in the genome-wide screen performed by Arita et al.,[1] they found that basal expression levels from their beta-estradiol inducible system were high enough that when certain essential genes were placed under inducible control, growth was permitted even in the absence of beta-estradiol. This promoted them to redesign their beta-estradiol system to reduce its level of basal expression. Thus, having multiple options, even for systems using the same inducer, can be very useful for researchers.
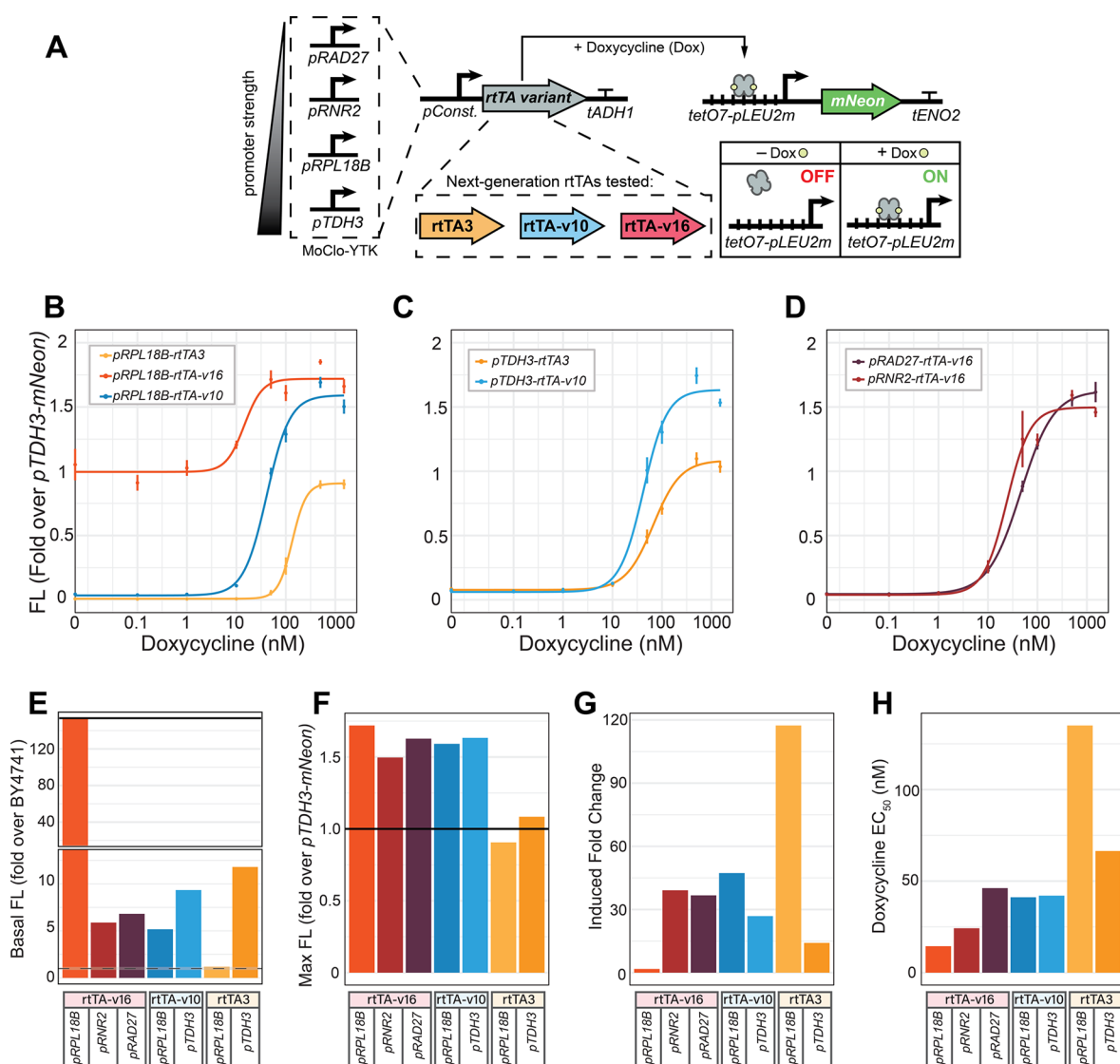
Figure 3. Design and induction properties of rtTA Dox-inducible systems. (A) The advanced rtTA variants rtTA3, rtTA-v10, and rtTA-v16 are tested by tuning their expression levels with MoClo-YTK promoters *pRAD27*, *pRNR2*, *pRPL18B*, and *pTDH3*. Binding of Dox to the rtTA variants allows them to bind to *tetO7-pLEU2m* and express the mNeon fluorescent reporter. (B) Induction curves of the three variants driven by *pRPL18B*. (C) Induction curves of rtTA3 and rtTA-v10 driven by *pTDH3*. (D) Induction curves of rtTA-v16 driven by *pRAD27* and *pRNR2*. Fluorescence (FL) values for each induction were normalized relative to mNeon fluorescence when constitutively expressed by *pTDH3* (*pTDH3-mNeon*). Circles represent mean values from *n* = 4 replicates, error bars represent standard deviation (SD), and fitted curves are shown as solid lines. (E) Basal FL levels of all tested rtTA systems expressed relative to the BY4741 strain not expressing any fluorescent protein. Mean BY4741 FL was normalized to 1 and is indicated by the dashed line. The shaded region represents one standard deviation above and below the mean. *pTDH3-mNeon* FL is indicated by the solid black line. (F) Maximal expression levels of each rtTA system expressed relative to *pTDH3*-mNeon (solid black line). (G) Fold change values for each rtTA system, calculated by dividing the maximal expression level by the basal expression level. (H) EC$_{50}$ values for each rtTA system, the Dox concentration at half-maximal expression, indicating the sensitivity of each system to Dox.[47]

ABA-Inducible Systems Based on ABI and PYL1 Chemically Induced Proximity. Having demonstrated that rtTA variants can be efficiently tuned in yeast with a MoClo-YTK-based approach, we wanted to use similar methods to design, build, and test ABA-inducible systems. ABA is a plant hormone that results in CIP and heterodimerization of the proteins ABI and PLY1.[31] Notably, Chang et al.[38] used these properties to create an ABA-inducible promoter system in CHO cells that exhibited induction properties similar to those of rtTA3. Their design utilized two constitutively expressed chimeric proteins. One consisted of PhlF, serving as the DB domain, fused to ABI as well as a nuclear export signal (NES), while the other protein contained a nuclear localization signal (NLS), PYL1, and the VP16 TA domain. Given the strong performance of this system in CHO cells, we reasoned that a similar performance could be achieved in yeast.

The design of our ABA-inducible promoter system generally followed the Chang et al.[38] organization of parts; however, in our system, ABI is fused to the NLS and TA domain and PYL1 is fused to PhlF-NES (Figure 4A). In order to modulate the induction properties of the ABA system, we tested three different activation domains, starting with VP48, which consists of three repeats of the minimal VP16 TA domain.[53] In this first configuration, a functional inducible promoter was built that responded to micromolar concentrations of ABA (Figure 4B,H), exhibited basal expression levels in the absence of ABA that were
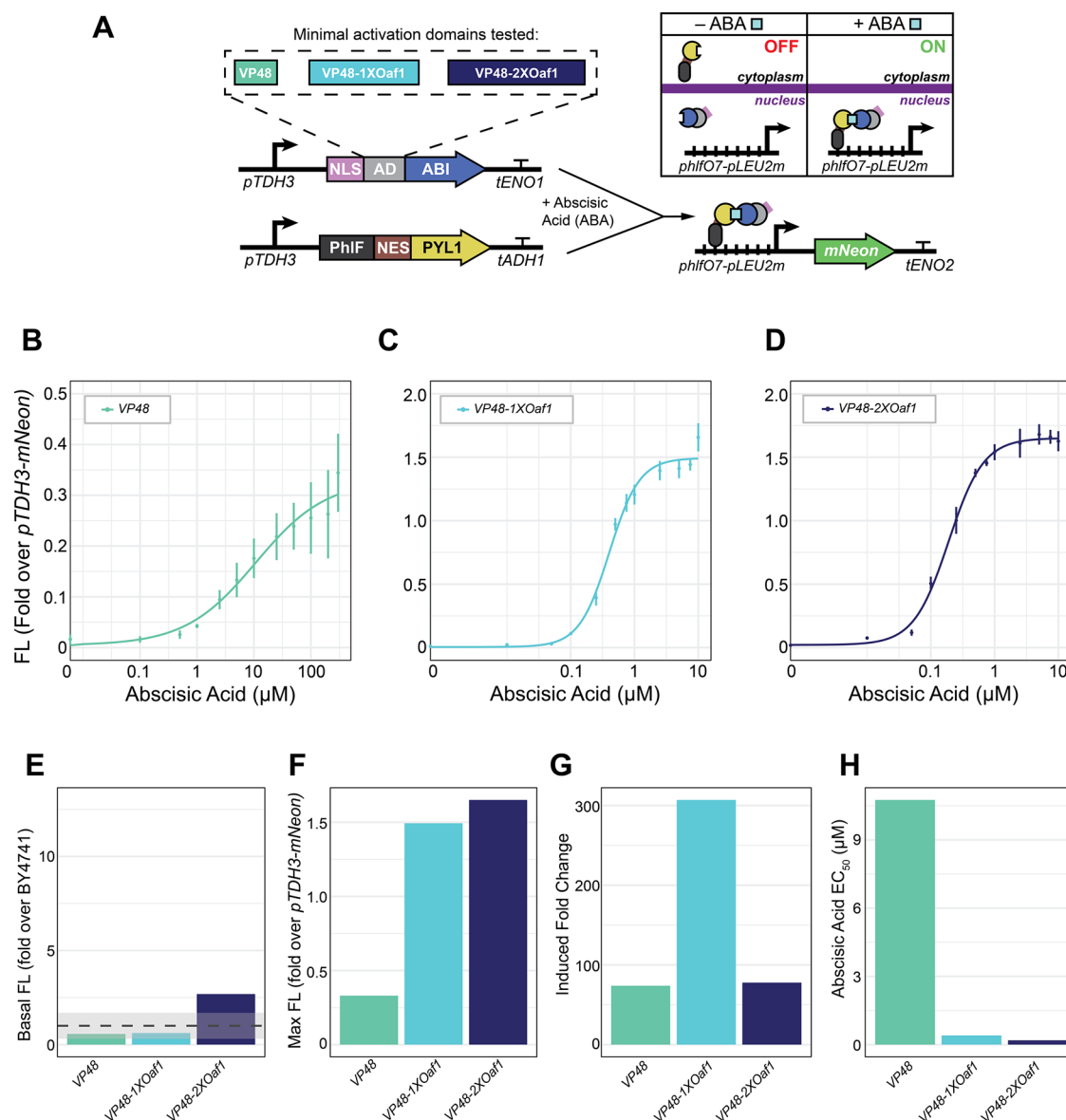
Figure 4. Design and induction properties of ABA-inducible systems. (A) Two fusion proteins, one composed of PhlF, an NES, and PYL1 and the other composed of an NLS, ABI, and a TA domain, were placed under the control of *pTDH3*. The NES on the PYL1 fusion protein promotes its export from the nucleus in the uninduced state, limiting its interactions with the ABI fusion protein, which harbors an NLS and localizes to the nucleus. For expression of mNeon, *pLEU2m* fused to seven repeats of the PhlF operator sequence (*phlf O7-pLEU2m*) was used. ABA promotes heterodimerization of the ABI and PYL1 chimeric proteins, allowing the complex to bind to *phlf O7-pLEU2m* and express mNeon. Three different activation domains were tested: VP48, VP48−1XOaf1, and VP48−2XOaf1. (B) Induction curve of the ABA system with VP48 as the activation domain. (C) Induction curve of the ABA system with VP48−1XOaf1 as the activation domain. (D) Induction curve of the ABA system with VP48−2XOaf1 as the activation domain. Fluorescence (FL) values for each induction were normalized relative to those of mNeon when constitutively expressed by *pTDH3* (*pTDH3*-mNeon). Circles are mean values from $n = 4$ replicates, error bars are SD, and fitted curves are shown as solid lines. (E) Basal FL levels of ABA systems with each of the three different activation domains tested and expressed relative to the BY4741 strain not expressing any fluorescent protein. Mean BY4741 FL (dashed line) was normalized to 1. The shaded region represents one SD above and below the mean. (F) Maximal expression levels of each ABA system expressed relative to *pTDH3*-mNeon. (G) Fold change values for each ABA system (maximum expression divided by basal expression). (H) EC_{50} values for each system.

virtually indistinguishable from BY4741 background fluorescence (Figure 4E), and had maximal expression that was 33% of *pTDH3*-mNeon (Figure 4B,F). Despite having maximal expression levels well below *pTDH3*-mNeon, the system had a ~74× fold change (Figure 4G) due to its low basal expression levels. The EC_{50} value of this system was 10.8 μM (Figure 4H).

Moving forward, we sought to increase the maximal expression levels of this system. Since the ABI and PYL1 components were already highly expressed by using the *TDH3*

promoter, we reasoned that we could improve this system by increasing the strength of the activation domain rather than tuning the promoters driving the components (as done with the Dox-inducible systems). To do this, we fused one or two copies of the activation domain of the yeast transcription factor Oaf1 to VP48, which we denote as VP48−1XOaf1 and VP48−2XOaf1 (Figure S3), respectively. We selected the Oaf1 activation domain because of its potency and compactness; a recent screen by Sanborn et al.[54] identified Oaf1 as having one of the strongest
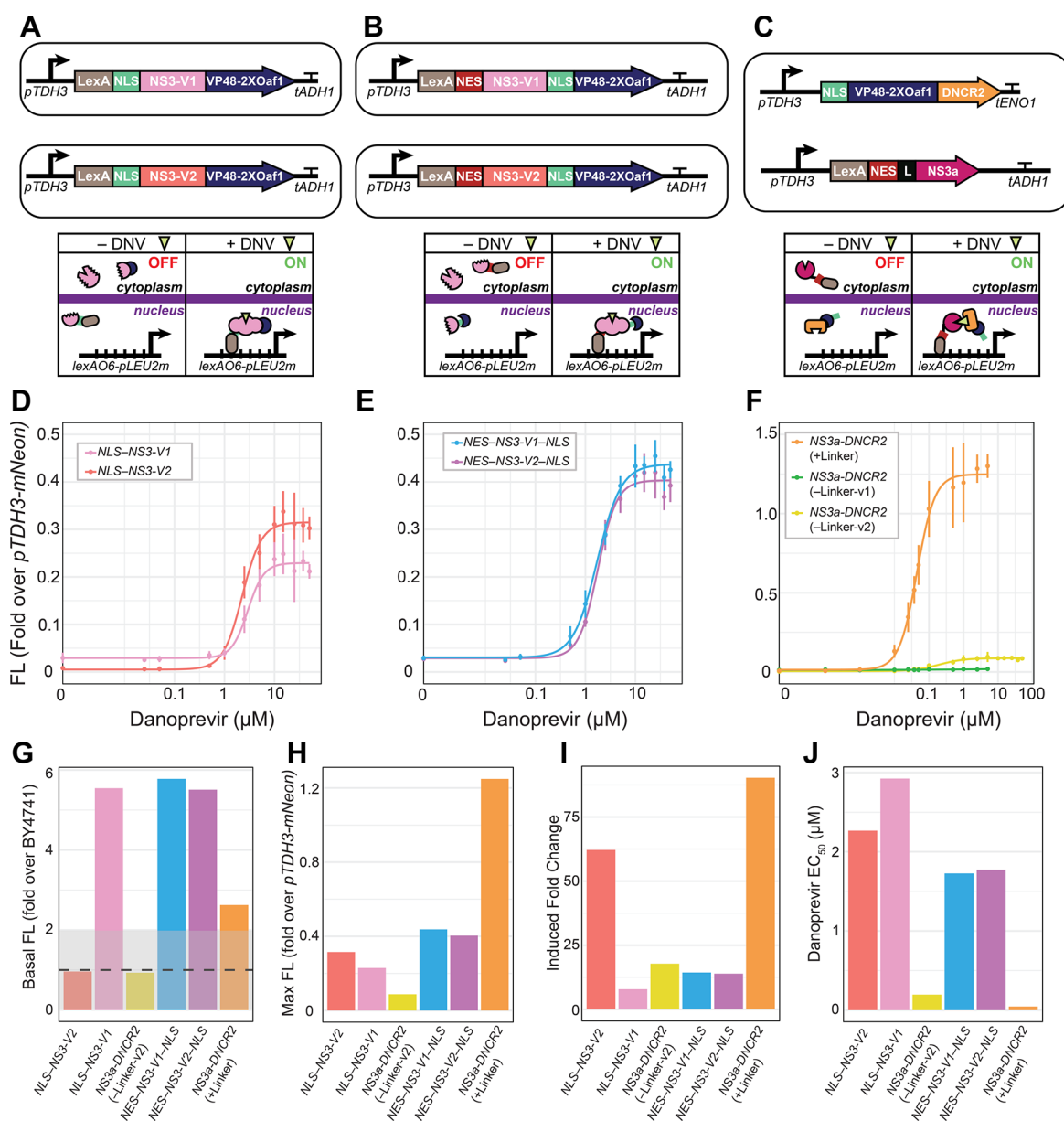
Figure 5. Design and induction properties of DNV-inducible systems. (A) Strains with the first NS3 transcription factors designed, which use LexA-NLS (from the Yeast GPCR-sensor Toolkit[23]) as the DB domain and VP48−2XOaf1 as the TA domain. NS3-V1 uses one NS5*A*/5B cut site and one NS4*A*/4B cut site flanking the NS3 protease, while NS3-V2 uses two NS4*A*/4B cut sites flanking the NS3 protease. Without DNV, the cleaved LexA-NLS translocates into the nucleus without the TA domain, but in the induced state with DNV, the intact transcription factor can bind to lexA operator sites and activate gene expression. (B) Strains with modified NS3-V1 and NS3-V2 inducible activators. An NES was placed on the LexA DB domain so that in the uninduced state it remains outside the nucleus. To allow mNeon induction in the presence of DNV, an NLS was placed between NS3 and the VP48−2XOaf1 TA domain. (C) Strain obtained using the NS3a-DNCR2 CIP system with a protein linker (L) on NS3a. NS3a and DNCR2 are separated between the cytoplasm and nucleus in the uninduced state via an NES on the LexA/NS3a fusion protein and an NLS on the DNCR2 fusion protein. DNV promotes the binding of NS3a and DNCR2 to activate gene expression in the nucleus. Three variants of this system were tested: one with a GGGSAGSGG linker attached to NS3a (+Linker) and two systems without the linker. For the systems without linkers, VP48−2XOaf1 TA domains were attached to DNCR2 (−Linker-v1) or to both DNCR2 and NS3a (−Linker-v2). (D) Induction curves for NS3-V1 and NS3-V2 designs using LexA-NLS and the DB domain (n = 7 replicates for NLS-NS3-V1, n = 5 replicates for NLS-NS3-V2). (E) Induction curves for NS3-V1 and NS3-V2 designs using LexA-NES as the DB domain and having an NLS preceding VP48−2XOaf1 (n = 4 replicates for each system). (F) Induction curves for NS3a-DNCR2 systems (n = 4 replicates for the −Linker-v1 variant, n = 3 replicates for the −Linker-v2 variant, and n = 5 replicates for the +Linker variant). For all induction curves, circular points are mean values, error bars are SD, and fitted curves are shown as solid lines. (G) Basal FL levels of each NS3 system expressed relative to the BY4741 strain not expressing any fluorescent protein. Mean BY4741 FL (dashed line) was normalized to 1. The shaded region is one SD above and below the mean. (H) Maximal expression levels of each NS3 system when induced by DNV. (I) Maximally induced fold change values. (J) EC_{50} values for all systems when induced with DNV.

TA domains in yeast, and it was previously shown to consist of just 27 amino acids in its C-terminus.[55,56] When the VP48−1XOaf1 and VP48−2XOaf1 variants were tested, we noted marked increases in not only the maximal expression levels reached but also the sensitivities to ABA (Figure 4C,D). Basal expression levels for VP48−1XOaf1 remained nearly identical to

the original ABA system using VP48 as well as to the background fluorescence levels measured for BY4741 (Figure 4E), while maximal levels were 1.5× higher than those of $pTDH3$-mNeon (Figure 4F), yielding a fold change of ~300× for this system and representing a more than 350% improvement in fold change relative to the ABA system using only VP48 (Figure 4G). For the VP48−2XOaf1 system, basal expression was 2.7× higher than BY4741 background levels (Figure 4E) and maximum expression was 1.7× that of $pTDH3$-mNeon (Figure 4F), resulting in a fold change of 77.8. In terms of sensitivity to ABA, when compared to the original VP48 system, the addition of 1XOaf1 or 2XOaf1 to the activation domain decreased the EC_{50} values by ~96 and 98%, respectively (Figure 4H). The EC_{50} of the VP48−2XOaf1 variant (~190 nM) was less than half that of the VP48−1XOaf1 variant (~403 nM).

From these results, it is clear that robust ABA-inducible promoters can be built in yeast and that tuning the strength of the activation domain allows a wide range of dose−response properties to be realized. Furthermore, by holding all parts of the system constant and only increasing the strength of the TA domain, we demonstrated that trade-offs can exist between maximal expression, sensitivity, and basal expression. While the addition of 1XOaf1 to VP48 dramatically improved the maximal expression and sensitivity at little cost to the basal expression levels, further improvement of VP48−1XOaf1 by adding an additional Oaf1 TA domain resulted in only a 10.5% increase in the max and 52.8% decrease in the EC_{50} but concomitantly increased the basal expression by more than 4×. These findings underscore the need for a multitude of easily customizable inducible systems to be made widely available, as it is unlikely that a single system possesses ideal characteristics across all performance metrics.

DNV-Inducible Systems Based on Controllable NS3 Proteolytic Cleavage and NS3a-DNCR2 Chemically Induced Proximity. To create a third class of inducible systems that were orthogonal to the rtTA and ABA systems, we set out to build upon work by Tague et al.[32] that used the NS3 serine protease from the hepatitis C virus (HCV) as the basis for constructing an inducible activator in mammalian cells. NS3 denotes a domain within the HCV nonstructural (NS) polyprotein that internally cleaves multiple recognition sites to produce the NS4 and NS5 proteins inside host cells.[57] Several antiviral small molecules, including danoprevir (DNV), asunaprevir (ASV), and grazoprevir (GZV), have been developed to block this critical step in HCV infection and work by binding to NS3 and inhibiting its proteolytic activity.[32,58,59] To create an inducible promoter system with these molecules, Tague et al.[32] designed a synthetic transcription factor with NS3 fused to a DB domain on its N-terminus and a TA domain on its C-terminus. Immediately flanking the NS3 domain are its two cleavage sites, termed NS4A/4B and NS5A/5B, which are cut in the absence of antiviral drugs, thereby stopping the association of the DB and TA domains of the transcription factor and preventing it from activating gene expression. However, when the antivirals are added to this system, they enable NS3 to act as a ligand-inducible connector, as cleavage at the NS4A/4B and NS5A/5B sites is inhibited and the intact transcription factor can successfully switch on gene expression.[32]

To port this system into yeast, we began by designing a Type 3B part that includes a yeast codon-optimized version of the NS3 domain and flanking NS4A/4B and NS5A/5B cut sites from Tague et al.[32] (Supporting Figure S4). We refer to this part

as NS3 version 1 (NS3-V1). For the TA and DB domains, we used VP48−2XOaf1 (validated for the aforementioned ABA system) and the bacterial LexA transcription factor from the Yeast GPCR-sensor Toolkit,[23] respectively (Figure 5A). Upstream of $pLEU2m$ driving the mNeon fluorescent reporter, we used lexAO6, featuring six copies of the LexA operator sequence, a Type 2A part that also came from the Yeast GPCR-sensor Toolkit[23] (as did $pLEU2m$). While this system successfully induced in yeast (Figure 5D), it displayed some undesirable induction characteristics; basal expression levels were more than five times that of the background BY4741 strain (Figure 5G) and because maximal expression values only reached 0.23 times that of $pTDH3$-mNeon (Figure 5H), a very modest fold change of 7.8 was obtained (Figure 5I). When alternative antiviral compounds, ASV and GZV, were tested, no improvements in the induction properties of the NS3-V1 system were observed (Figure S5). We note that we also tested an NS3-V1 system that used only the VP48 activation domain (as opposed to VP48−2XOaf1); however, this system did not successfully induce (data not shown). Since modifying the inducer did not enhance the maximal expression level or reduce the basal level, we sought other approaches to achieve these aims.

We reasoned that one possible explanation for the lower expression levels observed in the NS3 systems was that the protease activity of NS3 was not fully suppressed in yeast by DNV. Indeed, a similar observation was made by Chung et al.,[59] who created an NS3-based controllable degron system for protein tagging and degradation and found higher levels of NS3 proteolytic activity in yeast than in mammalian cells. However, the authors ameliorated this problem by using only the NS4A/4B cleavage site in their system, which is cut more slowly by NS3 than the NS5A/5B site, and noted that a potential reason why this change reduced basal expression in yeast when no such change was needed in mammalian cells was that the proteolytic activity of NS3 may be higher[59] at 30 °C than at 37 °C. Therefore, based on these findings, we constructed an NS3-V2 variant, where the NS5A/5B cut site has been removed and replaced with an NS4A/4B site, so that the NS3 protease is flanked on both sides by an NS4A/4B cut site. This change resulted in a more than fivefold reduction in basal expression as well as a 37.4% increase in the maximal expression level (Figure 3D,G,H). The fold change of the NS3-V2 system was 62.2, almost eight times higher than the fold change of the NS3-V1 system (Figure 5I). Finally, the DNV EC_{50} for NS3-V2 was reduced 22.5% relative to that of NS3-V1 (Figure 5J).

While the use of NS3-V2 resulted in improved performance, we wanted to explore possibilities for further increasing the maximal expression levels, especially since multiple Dox and ABA systems were able to induce to levels close to or above those of $pTDH3$-mNeon, while NS3-V2 only reached maximum levels that were around a third of $pTDH3$-mNeon. We decided to test how the arrangement of the system parts could affect the performance. In the original designs (Figure 5A), the NLS was fused to the LexA DB domain and was immediately downstream of an NS5A/5B (NS3-V1) or NS4A/4B (NS3-V2) cut site. Consequently, when the NS3 protease cleaves these locations, it results in a LexA-NLS component that can enter into the nucleus and bind to the lexAO sites of the promoter. We recognized that this had the potential to interfere with the induction properties of this system, since LexA-NLS components without AD domains could be occupying binding sites in the $lexAO6$-$pLEU2m$ promoter, even in the presence of DNV, assuming that some small amount of NS3 cleavage can occur even at the
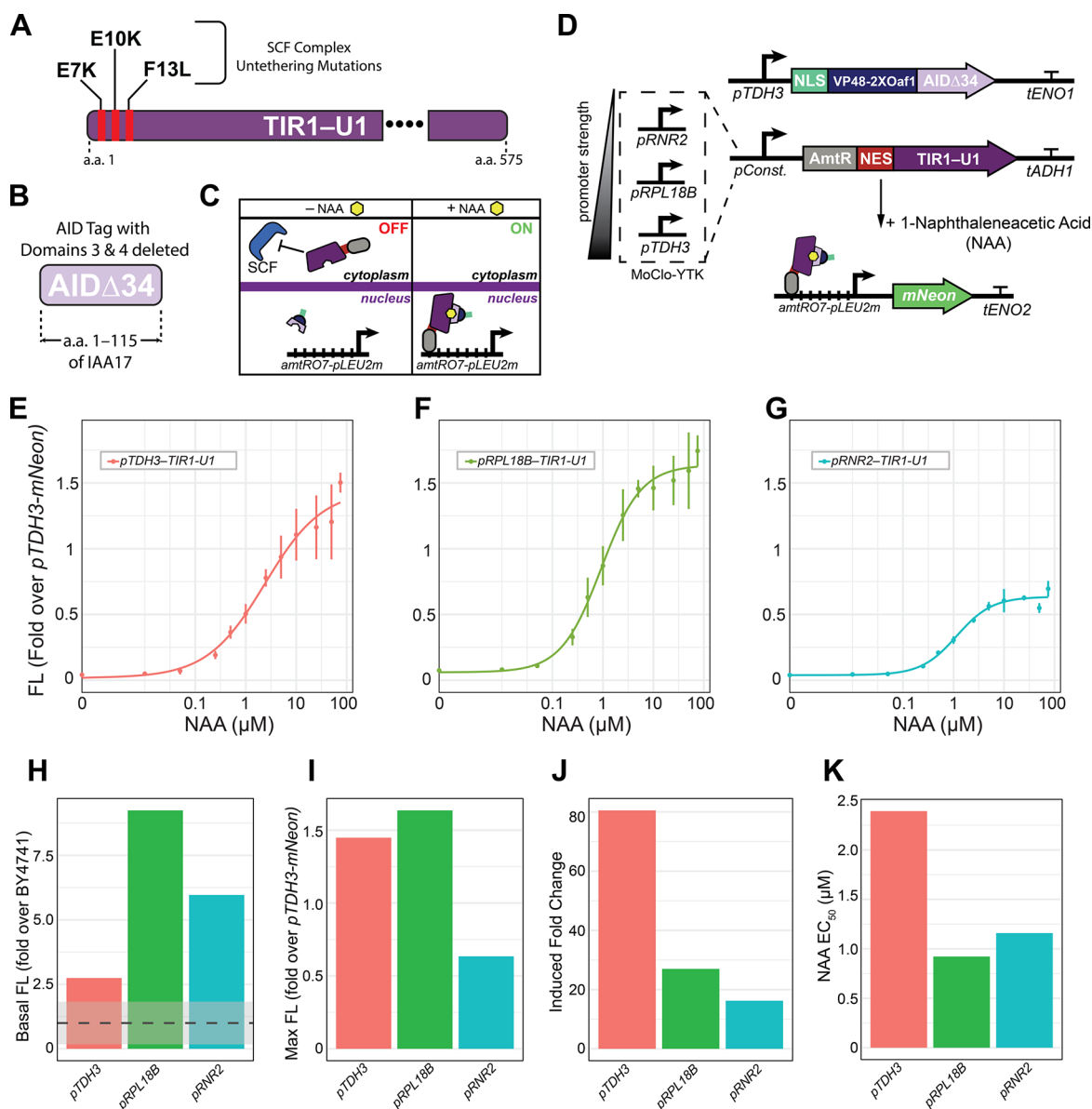
Figure 6. Design and induction properties of NAA-inducible systems. (A) Design of the TIR-U1 protein, featuring the E7K, E10K, and F13L mutations that untether it from the SCF complex, thereby abrogating the ubiquitination and degradation of AID-tagged proteins. (B) Design of AIDΔ34, the CIP binding partner of TIR-U1. AIDΔ34 consists of only the first 115 amino acids of the IAA17 protein, with its third and fourth protein domains deleted from this sequence. (C) Designed function of the NAA-inducible system. TIR-U1 is fused to an NES and AmtR DB domain, so that in the absence of NAA, it is localized to the cytoplasm but unable to assemble into an SCF complex as a result of the E7K, E10K, and F13L mutations. AIDΔ34 is fused to an NLS and VP48−2XOaf1 TA domain, which localizes to the nucleus. When NAA is added during the induction, TIR-U1 and AIDΔ34 bind to one another, forming a complete synthetic transcription factor that binds to *amtRO7-pLeu2m*. (D) Design of individual cassettes for the NAA-inducible system. (E) Induction curve of the *pTDH3*-AmtR-NES-TIR1-U1-driven variant. (F) Induction curve of the *pRPL18B*-AmtR-NES-TIR1-U1-driven variant. (G) Induction curve of the *pRNR2*-AmtR-NES-TIR1-U1 driven variant. Fluorescence (FL) values for each induction were normalized relative to mNeon when constitutively expressed by *pTDH3* (*pTDH3*-mNeon). Circles are mean values from $n = 4$ replicates for each variant strain, error bars are SD, and fitted curves are shown as solid lines. (H) Basal FL levels of NAA systems expressed relative to the BY4741 strain not expressing any fluorescent protein. Mean BY4741 FL (dashed line) was normalized to 1. The shaded region represents one SD above and below the mean. (I) Maximal expression levels of each NAA system expressed relative to *pTDH3*-mNeon. (J) Fold change values for each NAA system (maximum expression divided by basal expression). (K) EC_{50} values for each NAA system.

highest inducer concentrations. Therefore, we designed new variants where the NLS was fused to the VP48−2XOaf1 TA domain, and an NES was fused to LexA, so that it remained outside the nucleus in the uninduced state (Figure 5B). Interestingly, these changes did successfully increase the expression values for both the V1 and V2 NS3 variants (Figure 5E) and both reached maximum levels that were ∼0.4× those of *pTDH3-mNeon* (Figure 5H). This amounted to a 90.7%

increase in maximal expression for NS3-V1 and a 28% increase in maximal expression for NS3-V2. However, NS3-V1 basal expression levels increased by 4.2% and NS3-V2 basal expression levels increased by 472.8% (Figure 5G). Altogether, these modifications led to the fold change of NS3-V1 nearly doubling, the fold change of NS3-V2 being reduced more than fourfold (Figure 5I) and the sensitivities of each to DNV increasing (Figure 5J). These results suggest that in the

originally designed systems, the placement of the NLS on LexA did reduce maximal expression levels by binding up operator sites with LexA-NLS proteins that had no TA domain; however, these same effects also kept basal levels low in the uninduced state, particularly for NS3-V2.

In a final attempt to obtain a DNV-inducible system with maximal expression levels close to those of *pTDH3-mNeon*, we decided to test the NS3a and DNCR2 CIP system developed by Foight et al.[43] Here, DNCR2, a protein designed with the help of computational tools, binds to the NS3 protease, referred to as NS3a by the authors, only in the presence of DNV, and it was demonstrated that these proteins could be used to create an inducible promoter system in mammalian cells.[43] Initially, we tested this system in yeast and were able to obtain a functional inducible promoter system by including a VP48−2XOaf1TA domain on both the DNCR2 and NS3a fusion proteins, that is, NLS-VP48−2XOaf1-DNCR2 and LexA-NES-NS3a-VP48−2XOaf1, both of which were driven by *pTDH3* (Figure 5F, noted as the −Linker-v2 strain). Yet, only modest induction in response to DNV was realized (Figure 5F). We found that the version with a VP48−2XOaf1 TA domain attached only to the DNCR2 fusion protein did not noticeably induce in the presence of DNV (Figure 5F, noted as the −Linker-v1 strain). However, we discovered that we could dramatically improve this system by including the protein linker sequence[43] GGGSAGSGG on the Type 3B NS3a part, immediately downstream of the LexA-NES DB domain (Figure 5C). This system, referred to as NS3a-DNCR2 (+Linker), strongly induced to levels 1.2× that of *pTDH3-mNeon* (Figure 5F,H) and had low basal expression levels that were 2.6× higher than the background fluorescence of the BY4741 strain (Figure 5G). Consequently, the NS3a-DNCR2 (+Linker) system attained a fold change of 90.3 (Figure 5I), the highest among all NS3-based systems tested. Finally, the NS3a-DNCR2 (+Linker) system was also extremely sensitive to DNV levels, having an EC50 of 0.05 μM (Figure 5J) and requiring as little as 1 μM DNV to achieve maximal induction. Taken together, these results from all seven NS3 variants demonstrate that systems of this kind can function successfully in yeast but also underscore the fact that the specific genetic context in which inducible system components are arranged and assembled can dramatically affect their performance characteristics.

NAA-Inducible Systems Based on TIR1-U1 and AIDΔ34 Chemically Induced Proximity. To build a fourth inducible promoter system for yeast, we were inspired by work from Zhao et al.,[34] who built an auxin/IAA-inducible promoter system in mammalian cells by engineering the *Oryza sativa* TIR1 (osTIR1) and *Arabidopsis thaliana* IAA17 proteins. These two proteins are frequently used to create an inducible protein degradation system;[60] proteins targeted for degradation can be fused to domain II of the IAA17 protein[61] (often referred to as the auxin-inducible degron or AID tag,[60] but other IAA proteins can be used for degradation tags[62]), which, in the presence of auxin, is bound by TIR1, an F-box protein that interacts with the SCF complex.[63,64] This results in the AID-tagged protein being ubiquitinated and subsequently degraded. In order to transform the interaction between osTIR1 and AID into a system that could allow for inducible gene expression, rather than protein degradation, Zhao et al.[34] began by introducing two mutations into the osTIR1 protein, E7K and E10K, which corresponded to two amino acid positions in the *Arabidopsis thaliana* TIR1 protein (amino acids 12 and 15) that were shown by Yu et al.[65] to be critical for its participation in stable SCF complex

formation. Zhao et al.[34] showed that the E7K and E10K mutations in OsTIR1 significantly reduced degradation of the TIR1 and AID complex upon the addition of IAA. As the final step to create an inducible promoter system, they constructed an optimized AID tag to serve as the binding partner for their engineered TIR1; they refer to this protein as AIDΔ34, because it consists of only the first two domains of the IAA17 protein. When this AID tag was fused to a VP16 activation domain and TIR1 was fused to a GAL4 DB domain, this system strongly promoted inducible gene expression in CHO and human cells upon the addition of IAA to the media.[34]

We set out to emulate the design of the auxin-inducible system made by Zhao et al.[34] and test its performance in yeast. First, we built an osTIR1 variant that was designed to participate minimally in the SCF complex formation. In the study by Yu et al.,[65] three mutations in the *A. thaliana* TIR1 protein (AtTIR1) were found to dramatically reduce the degradation of IAA proteins, ostensibly via untethering TIR1 from the SCF complex: E12K, E15K, and F18L. Based on these findings, Zhao et al.[34] performed alignment between AtTIR1 and OsTIR1 protein sequences to identify that the E7K and E10K mutations in OsTIR1 should mimic the effects of the E12K and E15K mutations in AtTIR1. However, from the Zhao et al.[34] alignment, we also noticed that F18L in AtTIR1 should correspond to F13L in OsTIR1. Therefore, we synthesized a yeast codon-optimized osTIR1 variant including E7K, E10K, and F13L mutations, with the idea trying to limit TIR1 assembly into the SCF complex as much as possible. We refer to this protein as TIR1-unthethered-1, or TIR1-U1 (Figure 6A), since it incorporates three mutations into osTIR1 regions related to those identified by Yu et al.[65] in AtTIR1 that could untether it from the SCF complex. Finally, to create a CIP-binding partner for TIR1-U1, we designed an IAA17 protein consisting of just its first 115 amino acids, or its first two domains,[35,61] which we refer to as AIDΔ34 (Figure 6B) since domains 3 and 4 of IAA17 have not been included (this same name was given to the AID construct made by Zhao et al.;[34] however, in their case, a slightly shorter sequence length was used).

With the TIR1-U1 and AIDΔ34 parts in hand, we followed the design strategy used for creating the yeast ABA system by fusing an NES and DB domain to one component and an NLS and TA domain to the other, so that in the uninduced state, the two are separated across the cytoplasm and nucleus, with cytoplasmic TIR1-U1 minimally associated with the SCF complex (Figure 6C). The tetR homologue AmtR[18] was used as the DB domain, VP48−2XOaf1 was used as the TA domain, and initially *pTDH3* was used as the promoter for both halves of the system (Figure 6D). However, we also tested the effects of using *pRPL18B* and *pRNR2* to drive TIR1-U1 expression. For the inducer, we opted to use the synthetic auxin NAA instead of IAA, since IAA has been noted to produce toxic byproducts when exposed to blue light when recording GFP fluorescence.[33]

All three variants were strongly induced upon the addition of NAA to the media. The variant with *pTDH3* driving AmtR-NES-TIR1-U1 (Figure 6E) had low basal expression levels that were around 2.7× higher than the background BY4741 strain (Figure 6H), while also having maximal expression levels exceeding those of *pTDH3-mNeon* (Figure 6I). Interestingly, swapping out the *TDH3* promoter driving AmtR-NES-TIR1-U1 for *pRPL18B* or *pRNR2* also allowed for robust induction in response to NAA (Figure 6F and G, respectively); however, both of these systems displayed higher basal expression levels than when *pTDH3* was used (Figure 6H). This was the opposite
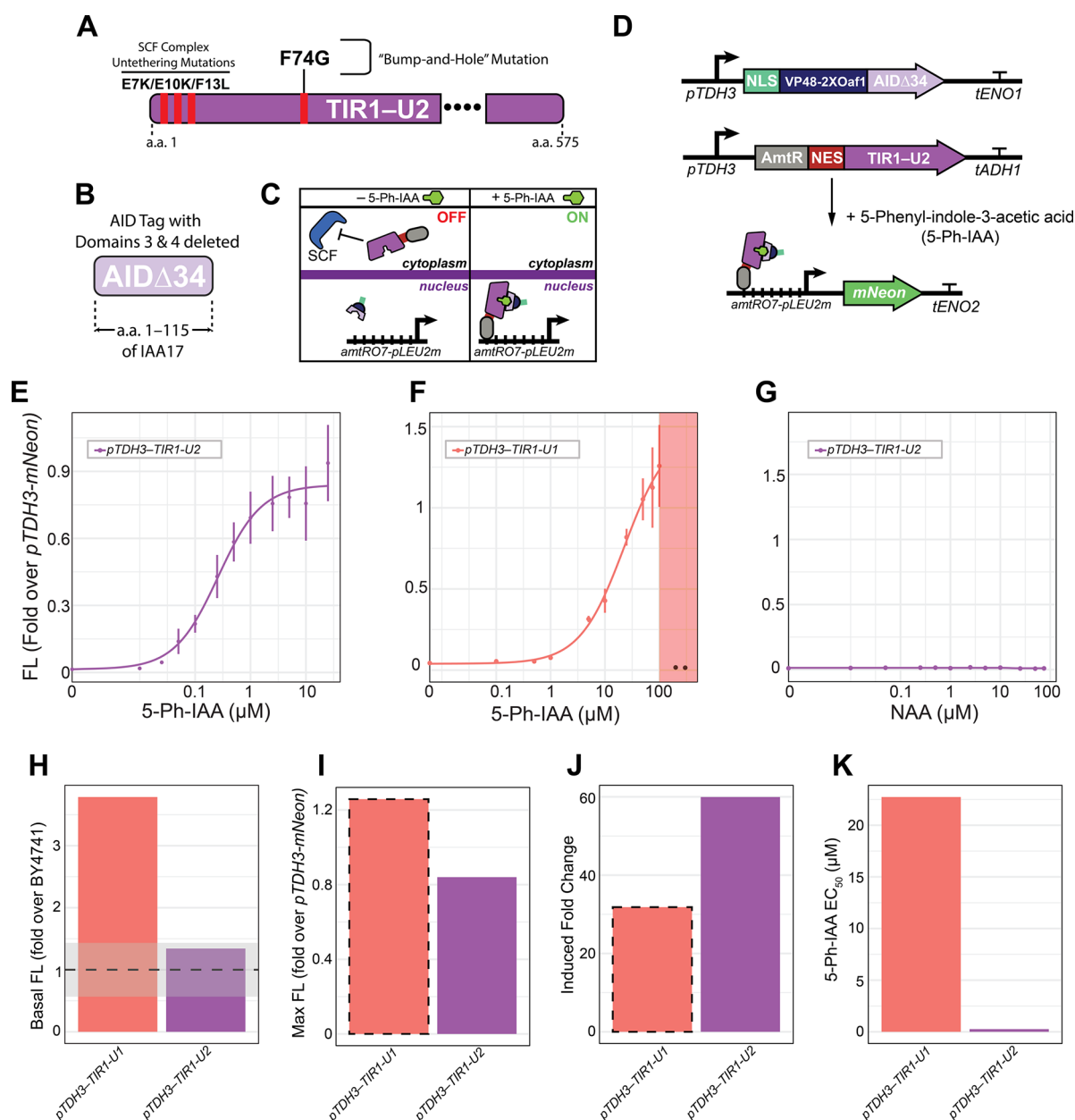
Figure 7. Design and induction properties of a 5-Ph-IAA-inducible system using TIR1-U2. (A) Design of the TIR1-U2 protein, containing the F74G mutation required for the "bump-and-hole" strategy,[37] as well as the E7K, E10K, and F13L SCF untethering mutations previously utilized for the TIR1-U1 system. (B) Design of the 115-amino-acid AIDΔ34 protein, the CIP-binding partner of TIR-U2. (C) Proposed operation of the 5-Ph-IAA-inducible system, which functions analogously to the TIR1-U1 system. (D) 5-Ph-IAA-inducible systems cassettes used, featuring TIR-U2 and AIDΔ34. (E) Induction curve of the TIR1-U2 system in response to 5-Ph-IAA (n = 4 replicates). (F) Induction curve of the *pTDH3* driven TIR1-U1 system in response to 5-Ph-IAA. The red-shaded region indicates where 5-Ph-IAA toxicity was observed at high concentrations. Black dots represent data points collected at highly toxic levels of 5-Ph-IAA that were not included when fitting the induction curve (n = 4 replicates). (G) Induction curve of the TIR1-U2 system in response to NAA (n = 3 replicates). Circles are mean values, error bars are SD, and fitted curves are shown as solid lines. (H) Basal FL levels of the TIR1-U1 and TIR1-U2 systems tested with 5-Ph-IAA as the inducer and expressed relative to the BY4741 strain not expressing any fluorescent protein. Mean BY4741 FL (dashed line) was normalized to 1. The shaded region represents one SD above and below the mean. (I) Maximal expression levels of the TIR1-U1 and TIR1-U2 systems expressed relative to *pTDH3*-mNeon. The dotted line around the bar for TIR1-U1 denotes that for this system, rather than using the max value obtained through the curve fitting, the maximum FL observed at 100 μM was used instead, because the max value obtained from the fitted curve was in a region where cellular toxicity from 5-Ph-IAA was observed. (J) Fold change values for each system. Dotted line for TIR1-U1 denotes that the fold change for this system was calculated by dividing the basal value obtained from the fitted curve by the maximum FL observed at 100 μM, rather than using the maximum calculated from the curve fitting. (K) EC$_{50}$ values for each system.

of the effect seen in tuning the Dox-inducible systems, where decreasing the strengths of the promoter always decreased basal expression (Figure 3E). In terms of maximal expression, the use of *pRPL18B* led to a 12.9% increase in the maximum relative to that when *pTDH3* was used, but the use of *pRNR2* led to a 56.2%

decrease in the maximum. However, as a result of the changes in basal expression, the *pTDH3*-TIR1-U1 system displayed the highest fold change of 80.5, compared to 27.0 for the *pRPL18B* variant and 16.2 for the *pRNR2* variant (Figure 6J). Last, the *pRPL18B* variant had the greatest sensitivity to NAA (Figure
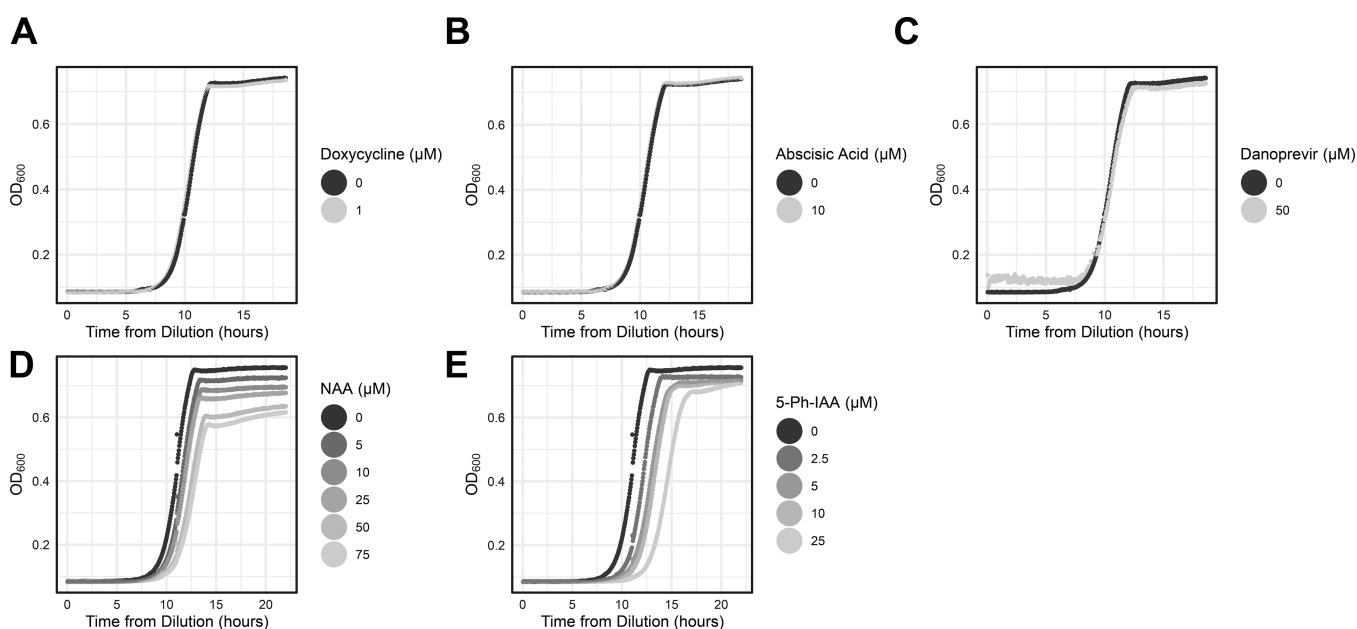
Figure 8. Inducer effects on long-term growth. (A) Strain growth with and without 1 μM Dox, the amount needed to induce maximal expression of the rtTA systems. (B) Strain growth with and without 10 μM ABA, the amount needed to induce maximal expression of the VP48−1XOaf1 and VP48−2XOaf1 variants of the ABI-PYL1 chemically induced proximity system. (C) Strain growth with and without 50 μM DNV, the amount needed to induce maximal expression of the NS3-V1 and NS3-V2 systems. (D) Strain growth with and without various concentrations of NAA, the inducer of the TIR1-U1 systems. (E) Strain growth with and without various concentrations of 5-Ph-IAA, the inducer of the TIR1-U2 system. In all cases, the BY4741 strain was used, and each condition contains at least n = 4 replicates, with the mean OD$_{600}$ values plotted for each condition.

6K). These results demonstrate the successful design and application of an NAA-inducible promoter system in yeast using the TIR1-U1 and AIDΔ34 proteins as a CIP system. Potential future studies could use the yTEST kit to further investigate the mechanisms underlying the observation that using the strong *TDH3* promoter was the most effective at limiting basal expression from this system.

5-Ph-IAA-Inducible Systems Based on TIR1-U2 and AIDΔ34 Chemically Induced Proximity. Having successfully developed an NAA-based inducible system using TIR1-U1 and AIDΔ34, we were intrigued about the possibility of applying the same design principles learned from these efforts to transform the recently reported AID2 protein degradation system[37] into a novel inducible promoter system. AID2 makes use of the "bump-and-hole"[66] modification for altering the association of TIR1 and IAA, where a mutation is introduced into TIR1 that alters its auxin binding pocket by creating a "hole" that only allows IAA molecules with modified indole rings or "bumps" to bind.[37,66] For OsTIR1, the F74G mutation introduces the "hole" needed for this approach, and Yesbolatova et al.[37] used this modified OsTIR1(F74G) variant to create the AID2 degradation system, which can inducibly degrade AID-tagged proteins upon the addition of 5-Ph-IAA, a synthetic auxin analog, to the media. This AID2 system was shown to exhibit reduced background degradation in the absence of an inducer, respond to significantly lower inducer concentrations than the original AID system with unmodified OsTIR1, and function in yeast, human cell lines, and even under *in vivo* conditions in mice.[37] Based on these impressive results, we sought to utilize this system for inducible gene expression.

To do this, we introduced the same F74G mutation used by Yesbolatova et al.[37] into our engineered TIR1-U1 protein, creating TIR1-U2 (Figure 7A). AIDΔ34 was unmodified and used as the CIP binding partner for TIR1-U2 (Figure 7B), allowing us to use the same design configuration and

arrangement of parts as previously used for the TIR1-U1 system and only requiring 5-Ph-IAA to be swapped in as the inducer (Figure 7C). As in the case of the TIR1-U1 system, AmtR and VP48−2XOaf1 were also used as the DB and TA domains, respectively, to enable direct comparisons and testing between the two systems (Figure 7D). The *TDH3* promoter drove both the TIR-U2 and AIDΔ34 cassettes since this promoter gave the highest fold changes when used with TIR1-U1.

When tested in yeast, the TIR1-U2 system was strongly induced in the presence of 5-Ph-IAA (Figure 7E). It maintained low basal expression levels nearly identical with the background BY4741 strain (Figure 7F) but exhibited high maximal expression levels nearly as strong (0.84×) as *pTDH3*-mNeon (Figure 7G), producing a maximum fold change of 60 for the TIR1-U2 system (Figure 7H). Furthermore, the system responded to 5-Ph-IAA with an EC$_{50}$ of 0.26 μM, making it more than nine times more sensitive to its inducer than TIR1-U1 is to NAA (EC$_{50}$ = 2.4 μM). For completeness, we tested the response of the TIR1-U1 system (*pTDH3* driven variant) to 5-Ph-IAA as well as the response of the TIR1-U2 system to NAA. We found that 5-Ph-IAA was able to promote inducible gene expression in the TIR1-U1 system, but only at extremely high concentrations (Figure 7F). In fact, substantial cellular toxicity was observed at 5-Ph-IAA concentrations higher than 100 μM (red-shaded region, Figure 7F). Despite this, TIR1-U1 was able to induce with 5-Ph-IAA to levels ~50% higher than those attained by TIR1-U2 (Figure 7I). Yet, its higher basal expression led to it having a maximum fold change of approximately half that of TIR1-U2 (Figure 7J). Finally, when NAA was tested as the inducer for the TIR1-U2 system, no induction was observed (Figure 7G).

In summary, we demonstrate here that the AID2 protein degradation system[37] can be re-engineered to operate as a robust inducible promoter system in *S. cerevisiae*. To the best of our knowledge, this TIR1-U2 CIP system for genetic regulation is
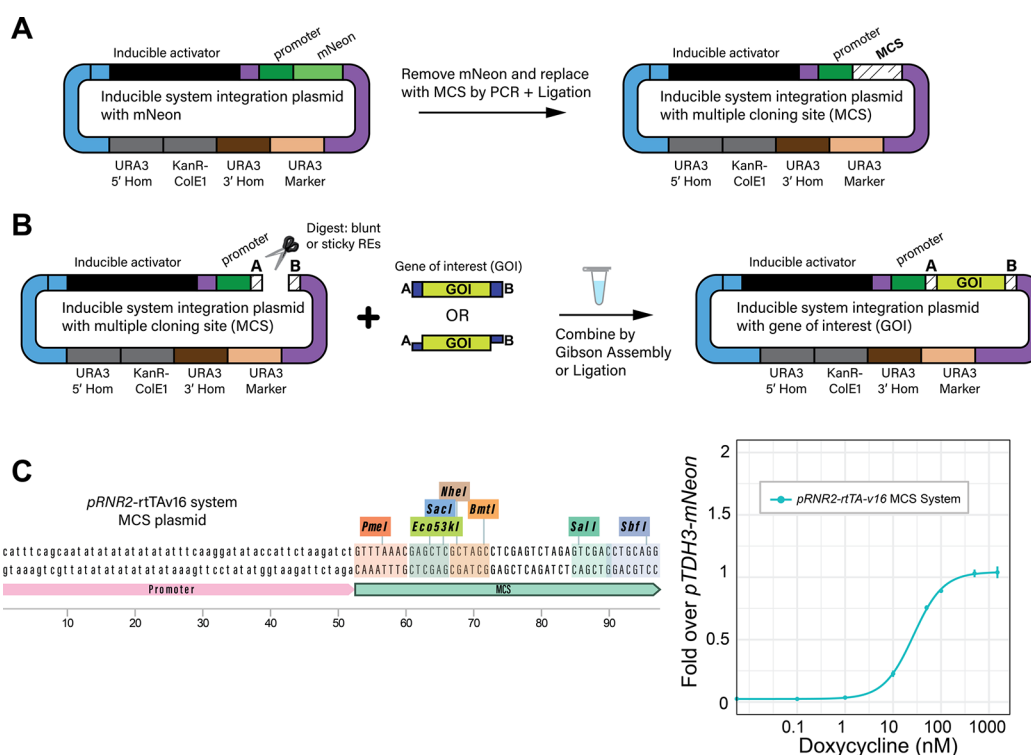
Figure 9. Construction and validation of MCS-inducible system integration plasmids. (A) For selected systems, mNeon was replaced in the multigene integration plasmid, which contained the inducible activator and promoter, and was replaced by an MCS. (B) MCS plasmids allow restriction enzymes (RE) that produce both blunt and sticky ends to be used to insert a gene of interest (GOI) into the plasmid so that its expression can be controlled by the upstream inducible system. Both Gibson Assembly and standard restriction−ligation cloning can be used to insert the GOI. (C) Design of a *pRNR2*-rtTAv16 MCS integration plasmid and validating its response to Dox by reinserting mNeon and testing its induction properties (*n* = 3 replicates). The DNA sequence image is a Benchling screenshot and was used with permission.

novel and has not been demonstrated before. Given that the AID2 system efficiently functions in human cell lines and mice,[37] the TIR1-U2 CIP system developed here could potentially be reoptimized for use in these higher eukaryotic systems, thereby expanding the ways in which gene expression can be controlled within mammalian cells.

Assessing the Effects of Sustained Exposure to yTEST Inducers on *S. cerevisiae* Growth. Having designed five inducible systems for yTEST that utilize five different inducers, we wanted to further investigate the effects that these inducers had on yeast growth. While we did not observe clear changes in strain growth during the 6 h induction experiments performed here (Supplementary Figure S7), we wanted to investigate how longer exposures to these inducers may affect yeast growth, in order to aid researchers in selecting optimal inducible systems and inducer concentrations for long-term experiments. To do this, we grew the BY4741 strain with and without the five yTEST inducers, using concentrations needed for maximal expression, and measured the OD_{600} values of the strains grown in each condition at 5 min intervals using a plate reader. We found that, qualitatively, 1 μM Dox (Figure 8A), 10 μM ABA (Figure 8B), and 50 μM DNV (Figure 8C), led to no noticeable growth changes. However, for NAA and 5-Ph-IAA, higher concentrations required for maximally inducing these systems resulted in reductions in strain growth (Figure 8D,E). Indeed, IAA was previously shown to inhibit growth in *S. cerevisiae* at very high concentrations in the millimolar range[67] (much higher than the micromolar concentrations used in this study). While decreasing the concentration of NAA to 5 μM and the concentration of 5-Ph-IAA to 2.5 μM could effectively mitigate these growth

changes (and these concentrations would still enable high induction levels from the TIR1-U1 and TIR1-U2 systems, respectively), these results demonstrate that careful consideration is warranted when choosing between different yTEST inducible systems for long-term experiments.

Multiple Cloning Site Plasmids for Rapid and Customizable Use of Inducible Systems. While yTEST includes the parts needed to assemble inducible systems and modify them to express genes of interest, we realized that some groups may want a simplified method for placing a gene of their choice under the control of an inducer. To address this, we also created versions of the multigene inducible system integration plasmids where a multiple cloning site (MCS) is included in place of mNeon (Figure 9A). These MCS integration plasmids make it simple to insert a desired gene by restriction-ligation cloning or Gibson Assembly (Figure 9B) and were done for the following systems: *pRNR2*-rtTAv16, *pRPL18B*-rtTA3, the ABA system with VP48−2XOaf1, and the NLS-NS3-V1 system (Supporting Figure S6).

To validate this approach, we reinserted mNeon into the pRNR2-rtTAv16 MCS integration plasmid by digesting the MCS plasmid with the blunt-end restriction enzyme *PmeI*, followed by a Gibson Assembly reaction to insert mNeon into the linearized plasmid. We then integrated the resulting construct into yeast and tested its behavior. As expected, we found that the *pRNR2*-rtTAv16 system was able to express mNeon upon the addition of Dox; however, we saw a smaller maximal response compared to the original plasmid system (Figure 9C). This is potentially due to changes in the 5′ UTR from leftover base pairs of the MCS. Existing research suggests

that modifications to the 5′ UTR can have significant impacts on gene expression levels from synthetic promoters in yeast.[68] Nonetheless, our results suggest that the MCS versions of the inducible system integration plasmids will be a useful tool for researchers who wish to quickly utilize an inducible system in yTEST to control the expression of a target gene in yeast.

SUMMARY

Inducible promoter systems are widely used by yeast researchers in both molecular and synthetic biology research. However, currently available systems are few in number and lack standardization. Here, we detail the development and characterization of yTEST, an extension of MoClo-YTK that includes parts for constructing yeast inducible promoter systems with broad ranges of dose responses to five different small-molecule inducers. Thus, by choosing different systems included in yTEST, different sensitivities to inducers as well as different basal and maximal expression levels can be achieved. This is a critical feature of this kit, as different applications can require very high expression levels of transgenes, digital or analog-like responses to inducers, or tight control of gene expression with minimal leakiness.

The yTEST kit presented here represents part of a growing list of MoClo-based kits with parts for CRISPR/Cas9 genome engineering,[69] optogenetics,[70] and signaling pathway modulation[23] in yeast. Notably, Sanford et al.[71] recently reported a MoClo kit for yeast that consists of both new and improved hormone-inducible systems controllable by beta-estradiol, testosterone, aldosterone, and 1,2-bis(4-hydroxyphenyl)-ethane-1,2-dione (DHB). Together, yTEST and the kit by Sanford et al.[71] provide a broad, diverse, and complementary set of inducible systems that can be utilized by yeast researchers for a wide range of applications. Moving forward, future work can further build upon and expand yTEST to include additional inducible promoter systems as well as other modes of inducible regulation. We also envision that a similar kit for small-molecule-controlled protein degradation could be designed for yeast, which could include auxin[37,61,62] and trimethoprim (TMP)[72] inducible protein degradation systems.

Ultimately, we designed and built yTEST with the goal of helping to expand what is possible in yeast synthetic biology. As more extensions of MoClo-YTK are developed, we expect that the accessible and plug-and-play nature of this assembly framework will result in many innovations that use and combine parts from different kits in unique ways. As a result, *S. cerevisiae* may become increasingly used for synthetic biology applications of the future.

METHODS

Yeast Strains and Transformations. The BY4741 strain (MATa *his3Δ1 leu2Δ0 met15Δ0 ura3Δ0*, from the Nan Hao Lab at UCSD) was used for all experiments. For transforming yeast strains with linearized cassettes, we used the "Super-High Efficiency" yeast transformation protocol by William Shaw (https://benchling.com/protocols/hYSdel7a/yeast-transformation-super-high-efficiency) with some minor changes made. Briefly, a single BY4741 colony from a YPD agar plate was inoculated with liquid YPD media and grown overnight at 30 °C. This culture was then diluted 1:50 into 50 mL of YPD the following day and grown at 30 °C for 5–6 h. After this growth period, cells were placed in 50 mL Falcon tubes and spun down in a centrifuge for 10 min at 2000 rpm. YPD media was then replaced with 25 mL of 0.1 M lithium acetate (LiOAc), and the pellet was resuspended, centrifuged again, and then resuspended in 1 mL of fresh 0.1 M LiOAc. From this 1 mL of cells in LiOAc, we used 100 μL for individual transformations, and this volume was aliquoted into Eppendorf tubes. To begin, 10 μL of salmon sperm carrier DNA (boiled for 8 min at 100 °C and then cooled on ice while cells were being centrifuged) was added to each tube of cells at room temperature (RT), and a half hour later, 900 μL of a mixture of 30% PEG-3350 (Sigma-Aldrich), 0.1 M lithium acetate, and 10% DMSO was added and mixed with cells by gently pipetting up and down. After resting at RT for a half hour, a heat shock at 42 °C for 14 min was done and then the cells were centrifuged for 2 min at 8000 rpm so that the transformation mix could be removed with a pipet. Then, cells were gently mixed with 250 μL of 5 mM calcium chloride and allowed to incubate at RT for 10 min before being plated on synthetic complete (SC) agar plates with the appropriate nutrient selection. After colonies were visible, they were restreaked onto YPD plates and yeast colony PCR was done to verify which colonies had been properly transformed. For creating −80 °C glycerol stocks of correctly transformed colonies, we followed the McClean lab protocol (https://openwetware.org/wiki/McClean:_Glycerol_stocks_(yeast)) and combined 900 μL of overnight yeast culture with 900 μL of 30% glycerol.

Golden Gate Assembly Protocol. For Golden Gate cloning, we followed the protocol established by Lee et al. for MoClo-YTK,[12] or used a custom protocol based off of the NEB Golden Gate Assembly protocol (https://www.neb.com/en-us/applications/cloning-and-synthetic-biology/dna-assembly-and-cloning/golden-gate-assembly). Generally, when following the MoClo-YTK protocol, we combined part plasmids at 20 fmol and used vector backbones at 10 fmol for Golden Gate assemblies. For 10 μL reactions, these components were added to PCR tubes with 0.5 μL of T7 DNA Ligase (New England BioLabs Inc. (NEB)), 1 μL of T4 DNA Ligase Buffer (NEB), and 0.5 μL of BsmBI-v2 or BsaI (both from NEB) and filtered dH$_2$O was added to reach the 10 μL volume. We used the following thermocycler protocol: digestion for 2 min at 42 °C and ligation for 5 min at 16 °C for 25 cycles, followed by a final digestion step for 10 min at 60 °C and a heat inactivation step for 10 min at 80 °C. When using the custom NEB-based protocol we used BsaI-HFv2 (20000 U/mL) at 37 °C and BsmBI-v2 (10000 U/mL) at 42 °C where appropriate, with durations for digestion and ligation (at 16 °C) both being 1 min for making part plasmids and 5 min for all other reactions; 100 cycles were done and then final digestions at 60 °C for 10 min and heat inactivation at 80 °C for 10 min were carried out.

Construction of Parts and Plasmids. yTEST parts were designed by sourcing the DNA sequences of needed parts from the literature or Addgene and then yeast codon optimizing them using the Integrated DNA Technologies (IDT) codon optimization tool if they were coding sequences. For each part type, the appropriate MoClo-YTK overhangs were added to the sequence. When needed, the sequence of a part was in certain cases changed from the codon-optimized version in order to remove restriction sites for BsmBI, BsaI, and NotI. These DNA sequences were then ordered as gBlocks from IDT or from Genewiz. Parts were then cloned into the MoClo-YTK entry vector pYTK001 by BsmBI-mediated Golden Gate assembly, transformed into DH5α *Escherichia coli*, and plated on chloramphenicol LB plates. Colonies on these plates were Sanger sequenced (Genewiz and Eton Bioscience) to verify the

presence of a correctly formed construct, and these plasmids were then used for assembly of inducible systems.

An exception to this approach was the construction of the Type 3B part for TIR1-U2. Here, we used the TIR1-U1 part (from OsTIR1 containing the E7K/E10K/F13L mutations) and performed substitution site-directed mutagenesis from the plasmid pWN050 (see Supplementary Table of Parts and Plasmids). The following primers were ordered as phosphorylated oligonucleotides from IDT: F−5′Phos-CGCATG-GAGCTGACTTTAACC, R−5′Phos-GTTTTCCTTTCACCGTCAGG. The PCR product was circularized by blunt-end ligation using T4 Ligase, DpnI digested, and transformed into DH5α E. coli. The transformed cells were plated on a chloramphenicol LB plate. Sanger sequencing was done to verify the successful introduction of the F74G mutation (i.e., changing the phenylalanine (F) codon TTT to a glycine (G) codon GGA). This plasmid containing TIR1-U2 (OsTir1 with the E7K, E10K, F13L, and F74G mutations) was then used for constructing 5-Ph-IAA-inducible genetic cassettes.

For single-gene cassettes, parts were assembled by BsaI Golden Gate reactions into the vector pYTK095 while multigene cassettes were formed from BsmBI Golden Gate reactions using pYTK096, the preassembled MoClo-YTK URA3 integration plasmid. DH5α competent cells were used to transform these constructs, and kanamycin or ampicillin selection on LB agar plates was used where appropriate. Colony PCR was used to verify correctly assembled cassettes, which were then grown in LB-containing ampicillin or kanamycin, and plasmids were miniprepped (Qiagen). RE digestion of the plasmids was performed to verify that the constructs were of the expected length.

Characterization of Inducible Promoters. For testing strains, colonies were first streaked out on YPD plates and grown at 30 °C. A protocol similar to those done by Lee et al.[12] and Shaw et al.[23] was followed. Colonies were added to 500 μL of SC media in 96-well plates (deep, round-bottom), covered with Breathe-Easier Sealing Film (Diversified Biotech), and grown at 30 °C overnight for approximately 18 h, shaking at 750 rpm on a Scilogex MX-M Microplate Mixer. After this time, cultures were diluted 1:100 in fresh SC media in deep-well 96-well plates and the respective small-molecule inducers were added at this time. Cells were grown for 6 more hours (at 30 °C and 750 rpm) in the presence of each inducer. Dox was diluted in water to 100×, the concentration needed in the most concentrated well, and then serially diluted and added to each well at 1:100 when doing the dilution. The central stock we worked off of was 2 mM Dox in water. ABA was diluted in SC with NaOH (for solubility), and then serial dilutions were made in SC+NaOH (so that NaOH levels were constant across all levels of inducer) and then added to the plates. The main stock used was 500 μM ABA in SC with 0.04% v/v 1 N NaOH. For DNV, NAA, and 5-Ph-IAA, 100 mM stocks were made in DMSO and these were used to make 100× stocks for experiments. This same approach was used to make stocks of ASV and GZV in DMSO.

After the 6 h induction and growth period, mNeon and OD600 levels were measured. To do this, we added 200 μL of culture from each well and added it to the well of a black-walled and clear bottom plate (Tecan). In addition, these plates also had wells with a strain expressing pTDH3-mNeonGreen, a BY4741 strain not expressing any fluorescent protein and blank SC media wells containing no yeast cells. These wells were also tested with each concentration of inducer. For wells with

BY4741 without a fluorescent protein, mNeon fluorescence values for all inducer concentrations were averaged together; this value was used to subtract a background strain fluorescence from the strains containing inducible systems (Figures S6 and S7). OD600 values were processed in the same manner, and mNeon fluorescence was divided by the OD600 for each strain. A Tecan Infinite 200 microplate reader was used to perform fluorescence measurements, and mNeon fluorescence was measured with an excitation value of 499 nm and an emission value at 533 nm.

Analysis of Induction Curves. To analyze induction curves for each inducible system, we used the DRC package[73] in R. First, we calculated mean fluorescence and OD for all blank media wells in the run. We then subtracted the mean blank fluorescence and OD from mean background (BY4741 strain) fluorescence and OD. For every other well, we then subtracted the mean blank fluorescence from that well's fluorescence, subtracted the mean blank OD from that well's OD, and divided that well's new fluorescence by its new OD. This is normalized fluorescence. Next, we calculated the mean normalized fluorescence for pTDH3-mNeonGreen (yRO163 strain) and divided each measurement by the mean normalized fluorescence for it. We then fit all measurements for each strain, across different concentrations of inducer, to a four-parameter log−logistic model, with terms for basal and max expression constrained to a minimum of 0. Finally, we extracted parameters for the hill coefficient, half-maximal dose (EC$_{50}$), maximum expression, and basal expression from the model. For plots where expression was displayed in terms of fold change over background, we divided each measurement by the normalized fluorescence for the background (BY4741 strain) instead of the normalized fluorescence for pTDH3-mNeonGreen (yRO163 strain). Fold change was calculated by taking the maximal expression level and dividing it by the basal expression level. All parameters for the fitted curves are included in the Supplement.

For each set of data points for a specific strain at each concentration of inducer, we ran Dixon's Q test using 99% confidence values.[74] The test was run after normalization, and points identified as outliers were removed from the data set, which was normalized again. This was done to exclude occasional data points that resulted from pipetting errors, where extremely small or large values were measured for a given induction data point. A complete list of the data points excluded from analysis by Dixon's Q test can be found in the Supplement.

Growth Curve Measurements. Yeast growth curves in the presence of inducers were performed following previously published methods from our group.[75] Briefly, BY4741 colonies were inoculated in 2 mL of SC media and grown overnight at 30 °C. The next day, cultures were diluted to an OD600 of ∼0.2 and 1 μL was added to 98 μL of SC media in a 96-well plate (Corning) for each condition. 1 μL of inducer was added to each well for each of the respective conditions. The plate was placed in a Tecan Infinite 200 PRO plate reader and grown with shaking at 30 °C with OD600 measurements taken every 5 min.

Creation of Inducible System Integration Plasmids with a Multiple Cloning Site. To create versions of the NS3-V1, ABA VP48−2XOaf1, pRNR2-rtTAv16, and pRPL18B-rtTA3 multigene, yeast-integration plasmids where the mNeon-Green CDS was replaced with an MCS sequence (GTTTAAACGAGCTCGCTAGCCTCGAGTCTAGA-GAGTCGACCTGCAGG), we PCR-amplified the plasmids with Q5 DNA polymerase (NEB) in a 50 μL reaction with the following primers: 5′- TCGAGTCTAGAGTCGACCTG-

CAGGtaactcgagagtgcttttaactaagaatta-3′ and 5′-GGCTAGC-GAGCTCGTTTAAACagatcttagaatggtatatccttgaaatata-3′. Following PCR amplification, Template DNA was removed by adding 1 μL of DpnI directly to PCR and incubating at 37 °C for 30 min. The PCR fragments were then run on an agarose gel and extracted. The linear, gel-extracted fragments were recircularized by ligation in a 10 μL reaction. 1 μL of DNA was mixed with 7 μL of H$_2$O, 1 μL of T4 Ligase Buffer, 0.5 μL of T4 PNK, and 0.5 μL of T4 DNA Ligase and incubated at 37 °C for 30 min followed by incubation at room temperature for 2 h. 5 μL of the ligation reaction mix was used to transform 100 μL of chemically competent DH5alpha *E. coli*. The MCS-containing plasmids were then verified by Sanger Sequencing.

To ensure that the MCS could be used to clone new genes into the inducible systems, we placed the mNeonGreen back into the pRO248-MCS plasmid using the MCS. The pRO248-MCS was digested with blunt-end restriction enzyme PmeI. 1 μg of DNA was digested in a 50 μL reaction. To create a linearized mNeonGreen CDS with Gibson-assembly compatible overhangs for assembly with the PmeI-digested pRO248-MCS plasmid, mNeonGreen was PCR amplified with Q5 DNA polymerase in a 50 μL reaction with the following primers: 5′-taccattctaagatctgtttatgGTTTCAAAAGGGGAG-3′ and 5′-cgaggctagcgagctcgtttttaGGATCCCTTATACAATTC-3′. This PCR product was digested with DpnI and then gel extracted. The mNeonGreen PCR product and PmeI-digested pRO248-MCS plasmid were mixed at a 3:1 molar ratio of insert to vector and assembled in a 10 μL Gibson Assembly reaction mix using Gibson Assembly Master Mix from NEB. The reaction was incubated at 50 °C for 1 h prior to transformation into chemically competent DH5alpha by heat shock. The final assembled plasmid was verified by Sanger Sequencing.

■ ASSOCIATED CONTENT

Ⓢ Supporting Information

The Supporting Information is available free of charge at https://pubs.acs.org/doi/10.1021/acssynbio.3c00184.

> Comparison of advanced rtTA variants used in this study; promoter characterization; design of activation domains; core components of the NS3 protease sequence[13] and variants designed for this study; induction of NS3-V1 system with alternative antivirals; multiple-cloning site (MCS) plasmids; background BY4741 strain growth vs. inducer concentration; background BY4741 strain fluorescence vs. inducer concentration (PDF)

> Parts, plasmids, and yeast strains (XLSX)

> Dixon Q test identified outliers excluded from analysis (XLSX)

> All curve fitting parameters for each system (XLSX)

■ AUTHOR INFORMATION

Corresponding Authors

Richard O'Laughlin − *Department of Bioengineering, University of California San Diego, La Jolla, California 92093, United States*; Present Address: Present address: Department of Neuroscience and Mahoney Institute for Neurosciences, Perelman School of Medicine, University of Pennsylvania, Philadelphia, Pennsylvania 19104, United States (R.O.); ● orcid.org/0000-0002-7552-5421; Email: rolaughl@eng.ucsd.edu

Jeff Hasty − *Department of Bioengineering, University of California San Diego, La Jolla, California 92093, United States; Department of Molecular Biology, School of Biological Sciences and Synthetic Biology Institute, University of California San Diego, La Jolla, California 92093, United States*; Email: jhasty@ucsd.edu

Authors

Quoc Tran − *Department of Molecular Biology, School of Biological Sciences, University of California San Diego, La Jolla, California 92093, United States*; Present Address: Present address: Molecular Engineering & Sciences Institute, Department of Electrical & Computer Engineering, University of Washington, Seattle, Washington 98195, United States (Q.T.).; ● orcid.org/0009-0004-3928-5493

Andrew Lezia − *Department of Bioengineering, University of California San Diego, La Jolla, California 92093, United States*; ● orcid.org/0000-0001-8068-8834

Wasu Ngamkanjanarat − *Department of Bioengineering, University of California San Diego, La Jolla, California 92093, United States*

Philip Emmanuele − *Department of Bioengineering, University of California San Diego, La Jolla, California 92093, United States*

Nan Hao − *Department of Bioengineering, University of California San Diego, La Jolla, California 92093, United States; Department of Molecular Biology, School of Biological Sciences and Synthetic Biology Institute, University of California San Diego, La Jolla, California 92093, United States*

Complete contact information is available at:
https://pubs.acs.org/10.1021/acssynbio.3c00184

Author Contributions

Notes

■ ACKNOWLEDGMENTS

■ REFERENCES

(1) Arita, Y.; Kim, G.; Li, Z.; Friesen, H.; Turco, G.; Wang, R. Y.; Climie, D.; Usaj, M.; Hotz, M.; Stoops, E. H.; et al. A genome-scale

yeast library with inducible expression of individual genes. *Mol. Syst. Biol.* **2021**, *17* (6), No. e10207.

(2) Blount, B. A.; Weenink, T.; Ellis, T. Construction of synthetic regulatory networks in yeast. *FEBS Lett.* **2012**, *586* (15), 2112−2121.

(3) Moon, T. S.; Lou, C.; Tamsir, A.; Stanton, B. C.; Voigt, C. A. Genetic programs constructed from layered logic gates in single cells. *Nature* **2012**, *491* (7423), 249−253.

(4) Nielsen, A. A.; Der, B. S.; Shin, J.; Vaidyanathan, P.; Paralanov, V.; Strychalski, E. A.; Ross, D.; Densmore, D.; Voigt, C. A. Genetic circuit design automation. *Science* **2016**, *352* (6281), aac7341.

(5) Redden, H.; Morse, N.; Alper, H. S. The synthetic biology toolbox for tuning gene expression in yeast. *FEMS Yeast Res.* **2015**, *15* (1), 1−10.

(6) Tominaga, M.; Nozaki, K.; Umeno, D.; Ishii, J.; Kondo, A. Robust and flexible platform for directed evolution of yeast genetic switches. *Nat. Commun.* **2021**, *12* (1), 1846.

(7) Chen, Y.; Zhang, S.; Young, E. M.; Jones, T. S.; Densmore, D.; Voigt, C. A. Genetic circuit design automation for yeast. *Nat. Microbiol* **2020**, *5* (11), 1349−1360.

(8) Ikushima, S.; Boeke, J. D. New Orthogonal Transcriptional Switches Derived from Tet Repressor Homologues for Saccharomyces cerevisiae Regulated by 2,4-Diacetylphloroglucinol and Other Ligands. *ACS Synth. Biol.* **2017**, *6* (3), 497−506.

(9) Aranda-Diaz, A.; Mace, K.; Zuleta, I.; Harrigan, P.; El-Samad, H. Robust Synthetic Circuits for Two-Dimensional Control of Gene Expression in Yeast. *ACS Synth. Biol.* **2017**, *6* (3), 545−554.

(10) McIsaac, R. S.; Oakes, B. L.; Wang, X.; Dummit, K. A.; Botstein, D.; Noyes, M. B. Synthetic gene expression perturbation systems with rapid, tunable, single-gene specificity in yeast. *Nucleic Acids Res.* **2013**, *41* (4), No. e57.

(11) McIsaac, R. S.; Silverman, S. J.; McClean, M. N.; Gibney, P. A.; Macinskas, J.; Hickman, M. J.; Petti, A. A.; Botstein, D. Fast-acting and nearly gratuitous induction of gene expression and protein depletion in Saccharomyces cerevisiae. *Mol. Biol. Cell* **2011**, *22* (22), 4447−4459.

(12) Lee, M. E.; DeLoache, W. C.; Cervantes, B.; Dueber, J. E. A Highly Characterized Yeast Toolkit for Modular, Multipart Assembly. *ACS Synth. Biol.* **2015**, *4* (9), 975−986.

(13) Giniger, E.; Varnum, S. M.; Ptashne, M. Specific DNA binding of GAL4, a positive regulatory protein of yeast. *Cell* **1985**, *40* (4), 767−774.

(14) Labbe, S.; Thiele, D. J. Copper ion inducible and repressible promoter systems in yeast. *Methods Enzymol* **1999**, *306*, 145−153.

(15) Nevoigt, E.; Kohnke, J.; Fischer, C. R.; Alper, H.; Stahl, U.; Stephanopoulos, G. Engineering of promoter replacement cassettes for fine-tuning of gene expression in Saccharomyces cerevisiae. *Appl. Environ. Microbiol.* **2006**, *72* (8), 5266−5273.

(16) Charvin, G.; Cross, F. R.; Siggia, E. D. A microfluidic device for temporally controlled gene expression and long-term fluorescent imaging in unperturbed dividing yeast cells. *PLoS One* **2008**, *3* (1), No. e1468.

(17) Deuschle, U.; Hipskind, R. A.; Bujard, H. RNA polymerase II transcription blocked by Escherichia coli lac repressor. *Science* **1990**, *248* (4954), 480−483.

(18) Stanton, B. C.; Siciliano, V.; Ghodasara, A.; Wroblewska, L.; Clancy, K.; Trefzer, A. C.; Chesnut, J. D.; Weiss, R.; Voigt, C. A. Systematic transfer of prokaryotic sensors and circuits to mammalian cells. *ACS Synth. Biol.* **2014**, *3* (12), 880−891.

(19) Das, A. T.; Tenenbaum, L.; Berkhout, B. Tet-On Systems For Doxycycline-inducible Gene Expression. *Curr. Gene Ther.* **2016**, *16* (3), 156−167.

(20) Gossen, M.; Bujard, H. Tight control of gene expression in mammalian cells by tetracycline-responsive promoters. *Proc. Natl. Acad. Sci. U. S. A.* **1992**, *89* (12), 5547−5551.

(21) Gossen, M.; Freundlieb, S.; Bender, G.; Muller, G.; Hillen, W.; Bujard, H. Transcriptional activation by tetracyclines in mammalian cells. *Science* **1995**, *268* (5218), 1766−1769.

(22) Louvion, J. F.; Havaux-Copf, B.; Picard, D. Fusion of GAL4-VP16 to a steroid-binding domain provides a tool for gratuitous induction of galactose-responsive genes in yeast. *Gene* **1993**, *131* (1), 129−134.

(23) Shaw, W. M.; Yamauchi, H.; Mead, J.; Gowers, G. F.; Bell, D. J.; Oling, D.; Larsson, N.; Wigglesworth, M.; Ladds, G.; Ellis, T. Engineering a Model Cell for Rational Tuning of GPCR Signaling. *Cell* **2019**, *177* (3), 782−796.e27.

(24) Bashor, C. J.; Patel, N.; Choubey, S.; Beyzavi, A.; Kondev, J.; Collins, J. J.; Khalil, A. S. Complex signal processing in synthetic gene circuits using cooperative regulatory assemblies. *Science* **2019**, *364* (6440), 593−597.

(25) Ren, G.; Ma, A.; Liu, W.; Zhuang, X.; Zhuang, G. Bacterial signals N-acyl homoserine lactones induce the changes of morphology and ethanol tolerance in Saccharomyces cerevisiae. *AMB Express* **2016**, *6* (1), 117.

(26) Troppens, D. M.; Dmitriev, R. I.; Papkovsky, D. B.; O'Gara, F.; Morrissey, J. P. Genome-wide investigation of cellular targets and mode of action of the antifungal bacterial metabolite 2,4-diacetylphloroglucinol in Saccharomyces cerevisiae. *FEMS Yeast Res.* **2013**, *13* (3), 322−334.

(27) Moullan, N.; Mouchiroud, L.; Wang, X.; Ryu, D.; Williams, E. G.; Mottis, A.; Jovaisaite, V.; Frochaux, M. V.; Quiros, P. M.; Deplancke, B.; et al. Tetracyclines Disturb Mitochondrial Function across Eukaryotic Models: A Call for Caution in Biomedical Research. *Cell Rep* **2015**, *10* (10), 1681−1691.

(28) Regehr, K. J.; Domenech, M.; Koepsel, J. T.; Carver, K. C.; Ellison-Zelski, S. J.; Murphy, W. L.; Schuler, L. A.; Alarid, E. T.; Beebe, D. J. Biological implications of polydimethylsiloxane-based microfluidic cell culture. *Lab Chip* **2009**, *9* (15), 2132−2139.

(29) Meyer, A. J.; Segall-Shapiro, T. H.; Glassey, E.; Zhang, J.; Voigt, C. A. Escherichia coli ″Marionette″ strains with 12 highly optimized small-molecule sensors. *Nat. Chem. Biol.* **2019**, *15* (2), 196−204.

(30) Endy, D. Foundations for engineering biology. *Nature* **2005**, *438* (7067), 449−453.

(31) Liang, F. S.; Ho, W. Q.; Crabtree, G. R. Engineering the ABA plant stress pathway for regulation of induced proximity. *Sci. Signal* **2011**, *4* (164), rs2.

(32) Tague, E. P.; Dotson, H. L.; Tunney, S. N.; Sloas, D. C.; Ngo, J. T. Chemogenetic control of gene expression and cell signaling with antiviral drugs. *Nat. Methods* **2018**, *15* (7), 519−522.

(33) Papagiannakis, A.; de Jonge, J. J.; Zhang, Z.; Heinemann, M. Quantitative characterization of the auxin-inducible degron: a guide for dynamic protein depletion in single yeast cells. *Sci. Rep* **2017**, *7* (1), 4704.

(34) Zhao, W.; Nguyen, H.; Zeng, G.; Gao, D.; Yan, H.; Liang, F. S. A chemically induced proximity system engineered from the plant auxin signaling pathway. *Chem. Sci.* **2018**, *9* (26), 5822−5827.

(35) Weijers, D.; Wagner, D. Transcriptional Responses to the Auxin Hormone. *Annu. Rev. Plant Biol.* **2016**, *67*, 539−574.

(36) Piotrowska-Niczyporuk, A.; Bajguz, A. The effect of natural and synthetic auxins on the growth, metabolite content and antioxidant response of green alga Chlorella vulgaris (Trebouxiophyceae). *Plant Growth Regulation* **2014**, *73* (1), 57−66.

(37) Yesbolatova, A.; Saito, Y.; Kitamoto, N.; Makino-Itou, H.; Ajima, R.; Nakano, R.; Nakaoka, H.; Fukui, K.; Gamo, K.; Tominari, Y.; et al. The auxin-inducible degron 2 technology provides sharp degradation control in yeast, mammalian cells, and mice. *Nat. Commun.* **2020**, *11* (1), 5701.

(38) Chang, M. M.; Gaidukov, L.; Jung, G.; Tseng, W. A.; Scarcelli, J. J.; Cornell, R.; Marshall, J. K.; Lyles, J. L.; Sakorafas, P.; Chu, A. A.; et al. Small-molecule control of antibody N-glycosylation in engineered mammalian cells. *Nat. Chem. Biol.* **2019**, *15* (7), 730−736.

(39) Li, H. S.; Israni, D. V.; Gagnon, K. A.; Gan, K. A.; Raymond, M. H.; Sander, J. D.; Roybal, K. T.; Joung, J. K.; Wong, W. W.; Khalil, A. S. Multidimensional control of therapeutic human cell function with synthetic gene circuits. *Science* **2022**, *378* (6625), 1227−1234.

(40) Gao, Y.; Xiong, X.; Wong, S.; Charles, E. J.; Lim, W. A.; Qi, L. S. Complex transcriptional modulation with orthogonal and inducible dCas9 regulators. *Nat. Methods* **2016**, *13* (12), 1043−1049.

(41) Bojar, D.; Scheller, L.; Hamri, G. C.; Xie, M.; Fussenegger, M. Caffeine-inducible gene switches controlling experimental diabetes. *Nat. Commun.* **2018**, *9* (1), 2318.

(42) Donahue, P. S.; Draut, J. W.; Muldoon, J. J.; Edelstein, H. I.; Bagheri, N.; Leonard, J. N. The COMET toolkit for composing customizable genetic programs in mammalian cells. *Nat. Commun.* **2020**, *11* (1), 779.

(43) Foight, G. W.; Wang, Z.; Wei, C. T.; Greisen, P., Jr; Warner, K. M.; Cunningham-Bryant, D.; Park, K.; Brunette, T. J.; Sheffler, W.; Baker, D.; et al. Multi-input chemical control of protein dimerization for programming graded cellular responses. *Nat. Biotechnol.* **2019**, *37* (10), 1209−1216.

(44) Stanton, B. Z.; Chory, E. J.; Crabtree, G. R. Chemically induced proximity in biology and medicine. *Science* **2018**, *359* (6380), No. eaao5902, DOI: 10.1126/science.aao5902.

(45) Wanke, V.; Cameroni, E.; Uotila, A.; Piccolis, M.; Urban, J.; Loewith, R.; De Virgilio, C. Caffeine extends yeast lifespan by targeting TORC1. *Mol. Microbiol.* **2008**, *69* (1), 277−285.

(46) Weber, E.; Engler, C.; Gruetzner, R.; Werner, S.; Marillonnet, S. A modular cloning system for standardized assembly of multigene constructs. *PLoS One* **2011**, *6* (2), No. e16765.

(47) Roney, I. J.; Rudner, A. D.; Couture, J. F.; Kaern, M. Improvement of the reverse tetracycline transactivator by single amino acid substitutions that reduce leaky target gene expression to undetectable levels. *Sci. Rep* **2016**, *6*, 27697.

(48) Urlinger, S.; Baron, U.; Thellmann, M.; Hasan, M. T.; Bujard, H.; Hillen, W. Exploring the sequence space for tetracycline-dependent transcriptional activators: novel mutations yield expanded range and sensitivity. *Proc. Natl. Acad. Sci. U. S. A.* **2000**, *97* (14), 7963−7968.

(49) Das, A. T.; Zhou, X.; Vink, M.; Klaver, B.; Verhoef, K.; Marzio, G.; Berkhout, B. Viral evolution as a tool to improve the tetracycline-regulated gene expression system. *J. Biol. Chem.* **2004**, *279* (18), 18776−18782.

(50) Zhou, X.; Vink, M.; Klaver, B.; Berkhout, B.; Das, A. T. Optimization of the Tet-On system for regulated gene expression through viral evolution. *Gene Ther.* **2006**, *13* (19), 1382−1390.

(51) Li, Y.; Jiang, Y.; Paxman, J.; O'Laughlin, R.; Klepin, S.; Zhu, Y.; Pillus, L.; Tsimring, L. S.; Hasty, J.; Hao, N. A programmable fate decision landscape underlies single-cell aging in yeast. *Science* **2020**, *369* (6501), 325−329.

(52) O'Laughlin, R.; Jin, M.; Li, Y.; Pillus, L.; Tsimring, L. S.; Hasty, J.; Hao, N. Advances in quantitative biology methods for studying replicative aging in Saccharomyces cerevisiae. *Transl Med. Aging* **2020**, *4*, 151−160.

(53) Cheng, A. W.; Wang, H.; Yang, H.; Shi, L.; Katz, Y.; Theunissen, T. W.; Rangarajan, S.; Shivalila, C. S.; Dadon, D. B.; Jaenisch, R. Multiplexed activation of endogenous genes by CRISPR-on, an RNA-guided transcriptional activator system. *Cell Res.* **2013**, *23* (10), 1163−1171.

(54) Sanborn, A. L.; Yeh, B. T.; Feigerle, J. T.; Hao, C. V.; Townshend, R. J.; Lieberman Aiden, E.; Dror, R. O.; Kornberg, R. D. Simple biochemical features underlie transcriptional activation domain diversity and dynamic, fuzzy binding to Mediator. *Elife* **2021**, *10*, No. e68068, DOI: 10.7554/eLife.68068.

(55) Baumgartner, U.; Hamilton, B.; Piskacek, M.; Ruis, H.; Rottensteiner, H. Functional analysis of the Zn(2)Cys(6) transcription factors Oaf1p and Pip2p. Different roles in fatty acid induction of beta-oxidation in Saccharomyces cerevisiae. *J. Biol. Chem.* **1999**, *274* (32), 22208−22216.

(56) Piskacek, S.; Gregor, M.; Nemethova, M.; Grabner, M.; Kovarik, P.; Piskacek, M. Nine-amino-acid transactivation domain: establishment and prediction utilities. *Genomics* **2007**, *89* (6), 756−768.

(57) Bartenschlager, R.; Ahlborn-Laake, L.; Mous, J.; Jacobsen, H. Nonstructural protein 3 of the hepatitis C virus encodes a serine-type proteinase required for cleavage at the NS3/4 and NS4/5 junctions. *J. Virol* **1993**, *67* (7), 3835−3844.

(58) Lin, M. Z.; Glenn, J. S.; Tsien, R. Y. A drug-controllable tag for visualizing newly synthesized proteins in cells and whole animals. *Proc. Natl. Acad. Sci. U. S. A.* **2008**, *105* (22), 7744−7749.

(59) Chung, H. K.; Jacobs, C. L.; Huo, Y.; Yang, J.; Krumm, S. A.; Plemper, R. K.; Tsien, R. Y.; Lin, M. Z. Tunable and reversible drug control of protein production via a self-excising degron. *Nat. Chem. Biol.* **2015**, *11* (9), 713−720.

(60) Nishimura, K.; Fukagawa, T.; Takisawa, H.; Kakimoto, T.; Kanemaki, M. An auxin-based degron system for the rapid depletion of proteins in nonplant cells. *Nat. Methods* **2009**, *6* (12), 917−922.

(61) Morawska, M.; Ulrich, H. D. An expanded tool kit for the auxin-inducible degron system in budding yeast. *Yeast* **2013**, *30* (9), 341−351.

(62) Khakhar, A.; Bolten, N. J.; Nemhauser, J.; Klavins, E. Cell-Cell Communication in Yeast Using Auxin Biosynthesis and Auxin Responsive CRISPR Transcription Factors. *ACS Synth. Biol.* **2016**, *5* (4), 279−286.

(63) Dharmasiri, N.; Dharmasiri, S.; Estelle, M. The F-box protein TIR1 is an auxin receptor. *Nature* **2005**, *435* (7041), 441−445.

(64) Kepinski, S.; Leyser, O. The Arabidopsis F-box protein TIR1 is an auxin receptor. *Nature* **2005**, *435* (7041), 446−451.

(65) Yu, H.; Zhang, Y.; Moss, B. L.; Bargmann, B. O.; Wang, R.; Prigge, M.; Nemhauser, J. L.; Estelle, M. untethering the TIR1 auxin receptor from the SCF complex increases its stability and inhibits auxin response. *Nat. Plants* **2015**, *1* (3), 14030 DOI: 10.1038/nplants.2014.30.

(66) Uchida, N.; Takahashi, K.; Iwasaki, R.; Yamada, R.; Yoshimura, M.; Endo, T. A.; Kimura, S.; Zhang, H.; Nomoto, M.; Tada, Y.; et al. Chemical hijacking of auxin signaling with an engineered auxin-TIR1 pair. *Nat. Chem. Biol.* **2018**, *14* (3), 299−305.

(67) Nicastro, R.; Raucci, S.; Michel, A. H.; Stumpe, M.; Garcia Osuna, G. M.; Jaquenoud, M.; Kornmann, B.; De Virgilio, C. Indole-3-acetic acid is a physiological inhibitor of TORC1 in yeast. *PLoS Genetics* **2021**, *17* (3), No. e1009414.

(68) Xu, L.; Liu, P.; Dai, Z.; Fan, F.; Zhang, X. Fine-tuning the expression of pathway gene in yeast using a regulatory library formed by fusing a synthetic minimal promoter with different Kozak variants. *Microb Cell Fact* **2021**, *20* (1), 148.

(69) Otto, M.; Skrekas, C.; Gossing, M.; Gustafsson, J.; Siewers, V.; David, F. Expansion of the Yeast Modular Cloning Toolkit for CRISPR-Based Applications, Genomic Integrations and Combinatorial Libraries. *ACS Synth. Biol.* **2021**, *10* (12), 3461−3474.

(70) An-Adirekkun, J. M.; Stewart, C. J.; Geller, S. H.; Patel, M. T.; Melendez, J.; Oakes, B. L.; Noyes, M. B.; McClean, M. N. A yeast optogenetic toolkit (yOTK) for gene expression control in Saccharomyces cerevisiae. *Biotechnol. Bioeng.* **2020**, *117* (3), 886−893.

(71) Sanford, A.; Kiriakov, S.; Khalil, A. S. A Toolkit for Precise, Multigene Control in Saccharomyces cerevisiae. *ACS Synth. Biol.* **2022**, *11* (12), 3912−3920.

(72) Gao, X. J.; Chong, L. S.; Kim, M. S.; Elowitz, M. B. Programmable protein circuits in living cells. *Science* **2018**, *361* (6408), 1252−1258.

(73) Ritz, C.; Baty, F.; Streibig, J. C.; Gerhard, D. Dose-Response Analysis Using R. *PLoS One* **2015**, *10* (12), No. e0146021.

(74) Dean, R. B.; Dixon, W. J. Simplified statistics for small numbers of observations. *Analytical chemistry* **1951**, *23* (4), 636−638.

(75) Baumgartner, B. L.; O'Laughlin, R.; Jin, M.; Tsimring, L. S.; Hao, N.; Hasty, J. Flavin-based metabolic cycles are integral features of growth and division in single yeast cells. *Sci. Rep* **2018**, *8* (1), 18045.